GEOLOGICAL SURVEY OF CANADA
OPEN FILE 6725

Electrical Geophysics Applied to Assessing Permafrost Conditions in Pangnirtung, Nunavut

G. A. Oldenborger

2010

Natural Resources Canada | Ressources naturelles Canada

Canada

GEOLOGICAL SURVEY OF CANADA
OPEN FILE 6725

Electrical Geophysics Applied to Assessing Permafrost Conditions in Pangnirtung, Nunavut

G. A. Oldenborger

2010

This publication is available from the Geological Survey of Canada Bookstore (http://gsc.nrcan.gc.ca/bookstore_e.php).
It can also be downloaded free of charge from GeoPub (http://geopub.nrcan.gc.ca/).

Recommended citation
Oldenborger, G. A., 2010. Electrical Geophysics Applied to Assessing Permafrost Conditions in Pangnirtung, Nunavut; Geological Survey of Canada, Open File 6725, 39 p.

Open files are products that have not gone through the GSC formal publication process.

TABLE OF CONTENTS

INTRODUCTION

As part of the project "Building Resilience to Climate Change in Canadian Communities" within the Climate Change Geoscience Program of Natural Resources Canada, electrical geophysical experiments were conducted in and around the hamlet of Pangnirtung, Nunavut in August 2009. Two-dimensional electrical resistivity imaging was performed in an effort to aid permafrost characterization and landscape hazard mapping efforts in the small Inuit community on Baffin Island. The electrical geophysical data were collected in conjunction with georadar data, geomorphologic mapping and shallow borehole drilling (see LeBlanc et al., 2010). The geophysical data are more extensive, spatially continuous, and provide deeper subsurface information than the mapping and drilling data. However, the geophysical data provide proxy measurements of geology and permafrost conditions, and are thus subject to interpretation and should be considered as complementary to other forms of terrain and permafrost assessment.

ELECTRICAL GEOPHYSICS

Low-frequency or direct-current (DC) electrical resistivity has been a well-established geophysical exploration tool for many years. The basic principle involves application of an active current source and mapping of the associated electrical potential field and its perturbation by geophysical targets or anomalies (Figure 1). The primary physical parameter governing the distribution of the electrical potential field is the electrical conductivity. Geophysical targets are thus defined by their relative electrical conductivity. Electrical conductivity is the most variable physical property of solid earth materials, easily spanning more than 10 orders of magnitude for rocks and sediments (e.g., Telford et al., 1990, p. 290).

In most geologic environments, electrical current is considered to propagate via electrolytic conduction or ionic conduction through pore fluids. Controlling factors on the electrical conductivity of rocks or sediments are the amount of pore fluid (porosity), the connectivity of the pore fluid (saturation), the availability and mobility of charge-carrying ions, and the material type inasmuch as it affects both the porosity and the availability and behaviour of ions in solution (e.g., McNeil, 1980; Klein and Santamarina, 2003). Permafrost is associated with a strong, but complicated electrical signature because variations in temperature and the liquid/solid phase transition of water strongly affect all the above factors (Figure 2).

The freezing of water reduces the available pore fluid and its connectivity. At low ground temperatures, the unfrozen water content is reduced to a point where there is little contrast in conductivity between frozen sediment or massive ice or even air (Hoekstra et al., 1975). At the same time, exclusion of salts from the solid phase typically increases ionic concentrations, but low temperatures reduce ionic mobility. At very low moisture contents or salinities, membrane polarization becomes significant and conductivity may be complex and dispersive. However, Pandit and King (1979) show that for moderate porewater salinity (>5 g/L NaCl) *or* temperatures near or above freezing, conductivity is primarily in-phase (non-polarized) and non-dispersive indicating dominantly ionic conduction in the (albeit small amount of) unfrozen water. As such, the non-complex electrical conductivity can generally be used to infer some combination of the

moisture content and the pore fluid conductivity, or similarly, the amount of frozen water and the material type.

GEOLOGICAL CONTEXT

Pangnirtung is a community on the southern shore of Pangnirtung Fjord on Baffin Island (Figure 3). Much of the geological context for geophysical survey design was based on prior work in Pangnirtung by geotechnical consultants. Near the Duval River crossing, a geotechnical report prepared by AMEC (Hsieh and Tchekhovski, 2008, not for release) indicates fluvial deposits of coarse sands and gravel with cobbles and boulders (up to 2 m) to approximately 14–17 m depth. These sands and gravels are underlain by marine silts and silty sands. The sands have moisture contents of approximately 7–10% and the marine sediments have moisture contents of 11–17%. Bedrock was not encountered at depths of 20 m. Pullan et al. (1998) provide some estimate of depth to bedrock based on seismic reflection experiments performed along the tidal flat of Pangnirtung. To the northeast near Mount Duval, depth to bedrock near shore is approximately 25 m. To the southwest near the airport, depth to bedrock near shore is approximately 10 m.

The geotechnical report by Thurber Consultants Ltd. (Isherwood, 1983, not for release) indicates that away from the Duval River, surficial sediments are marine deltaic silts, sands and gravels. Occurrences of thin peat (up to 1 m) are reported near the airport and reservoir. Near the airport, the peat occurs over 1.5–6 m of silts and clays with significant excess ice over ice-poor sands and gravels. Near the reservoir, a thin layer of peat occurs over an ice-rich coarse till, which in turn overlies a saturated, but ice-poor silty till (Smith et al., 1989).

Hyatt (1992) provides information on the first 6 m of surficial sediment from a cross-valley ground moraine on the southwest slope of Mount Duval. The upper diamicton is approximately 2 m thick and ice-poor; it is largely within the active layer (0.8–1.6 m) and has relatively low pore fluid conductivity and low silt/clay content. The lower diamicton is ice rich and completely below the active layer, but the conductivity of the pore fluid is higher than that of seawater (>10 S/m).

The available geological information suggests that although the hamlet of Pangnirtung is relatively small in area, it may exhibit significant variability in terrain conditions. This observation is supported by the geomorphologic work conducted as part of this study that indicates a zonal distribution of alluvium, colluvium, till and marine sediments (Carbonneau and Allard, 2009; Carbonneau et al., 2009; Leblanc et al., 2010). Bouldery gravels with low moisture content will be highly resistive, even above freezing. Conversely, marine sediments may be highly conductive even when frozen due to high salinity and/or clay content (e.g., Ross et al., 2007). Similarly, a diamicton below the active layer has the potential to be highly conductive given Hyatt's reported salinity. If the conductivity of the pore fluid decreases at depth, or the ice content increases, the bulk conductivity could decrease substantially (e.g., Scott et al., 1990).

DATA ACQUISITION

The bulk of the electrical surveys were carried out using a capacitively-coupled resistivity meter (Geometrics OhmMapper). In a capacitively-coupled resistivity (CCR) survey, current is generated in the ground via coupling of an alternating current across a transmitter-earth capacitor (Kuras et al., 2006). Similarly, voltage is measured via coupling of the resulting potential field across an earth-receiver capacitor. A CCR system such as the OhmMapper is non-contacting and allows for acquisition of data where physical contact with the ground via electrodes is prohibitive, such as along hamlet roads (Figure 4a) or where contact resistance with the ground is prohibitively high such as for ice or very dry soils. The OhmMapper can also be used off-road with relatively rapid acquisition.

Initial survey areas were targeted based on hazard identification (along the Duval River) and community planning (Phase 2 development area). As fieldwork proceeded, survey areas were targeted based on the geophysical data, the borehole data, geographic coverage and the evolving conceptual model. At the end of the deployment, complementary data were collected at select sites using a multi-electrode galvanic resistivity meter (IRIS Syscal R1+ Switch 48). The more traditional galvanic resistivity (GR) survey involves injection of current directly into the ground via galvanic contact with a pair of current electrodes (Figures 1 and 4b). The potential distribution is then measured across many pairs of voltage electrodes.

Capacitively-Coupled Resistivity

CCR data were collected using a six-dipole setup: one transmitter and five receivers. Initial surveys were executed with both 5 m and 10 m antenna lengths. Three passes were made with the 5 m and 10 m antennas, both at dipole spacings of n = 0.5, 1.0, 1.5, 2.0, 2.5; n = 3.0, 3.5, 4.0, 4.5, 5.0; and n = 5.0, 5.5, 6.0, 6.5, 7.0 (Figure 5a). Note that the reported nominal dipole n spacing is with respect to the antenna length and not any corrected equivalent dipole length for a line antenna (e.g., Kuras et al., 2006). Some dipole spacings were overlapped for data redundancy based on previous experience with high noise levels for OhmMapper data. However, redundant data proved to be problematic for subsequent inversions, which is an indication of poor repeatability.

Early in the deployment, a receiver was damaged and subsequent surveys were implemented with four receivers at dipole spacings of n = 0.5, 1.0, 1.5, 2.0; n = 3.0, 3.5, 4.0, 4.5; and n = 5.0, 5.5, 6.0, 6.5. Since overlapping dipole spacings resulted in inconsistent data and large n-spacing data were extremely noisy, no critical loss of information resulted from the loss of one receiver. Furthermore, an additional modification was the execution of only a single pass with the 10 m antennas at dipole spacings of n = 3.0, 3.5, 4.0, 4.5, 5.0. This resulted in a smoother transition of investigation depths from the three 5m dipole passes to the 10 m dipole pass and further mitigated the problem of inconsistent data during inversion.

In most cases, walk-away testing indicated that signal loss was prohibitive at transmitter-receiver separations in excess of 25 m for 5 m dipoles and 40 m for 10 m dipoles (from antenna end-to-end). This was surprising for permafrost terrain and was indicative of relatively conductive conditions. In some cases, only 5 m dipoles were used due to signal loss.

Surveys were conducted in the following order at the following sites. Line locations are identified in Figure 6:

Line 01, River: eastern bank of the Duval River, up-slope
Line 01x, River: eastern bank of the Duval River, cross-slope
Line 02, Phase 2: Phase 2 Area of the Pangnirtung community plan, cross-slope
Line 03, Reservoir Road: roadway below current reservoir, cross-slope
Line 04, Phase 2: western Phase 2 Area, up-slope
Line 05, Runway: roadway north of and parallel to airport runway
Line 06, Tower: radio tower slope behind the airport, up-slope
Line 07, SDH-05: Borehole 5 slope behind the airport, upslope
Line 08, Park: across the park in the western end of the hamlet
Line 09, Sewage Road: roadway along Phase 2 past the sewage plant
Line 10, Reservoir-River Road: roadway from the reservoir road to the river
Line 11, Phase 2 BH: eastern Phase 2 Area through DDH-02, up-slope
Line 12, Arena Road: roadway from the school to the campground past the arena

Galvanic Resistivity

To complement borehole sampling and the CCR data, approximately 1000 m of GR data were collected over three sites: Line 01, Line 11, and Line 08. Data were collected using 2 m and 3 m electrode spacings with 0.3 m stainless steel electrodes. A Wenner survey geometry was used to maximize signal strength in the permafrost environment. The 48-electrode data set consists of 360 measurements at depth spacing of 1 to 15 (Figure 5b). All surveys were performed with 1 s pulse duration with a minimum of 3 stacks and rolled in sections of 24 electrodes. Time-domain induced polarization (IP) and reciprocal data were collected for at least the first deployment of each line (before roll-along). Contact resistances were typically low to moderate (0.5–5 kΩ). Electrodes were treated with a saline solution if contact resistance was observed to be above 5–10 kΩ. In some locations along Line 08, contact resistances were observed to be in excess of 20 kΩ indicating that surface resistivity may be high and current injection may be limited.

PROCESSING AND INVERSION

All data processing begins with a thorough examination of the data and field notes and the elimination of any obvious outliers. Given satisfactory data, the initial processing step is assignment of survey geometry. The procedure is slightly different for CCR versus GR data, but the basic elements are the same: translation to a prescribed coordinate system and assignment of topography. In the case of 2D electrical data, we process in terms of survey lines and distance along the ground. For each line, we georeference the approximate start and end, or marker positions along each line. All data are translated such that the line position of 0.0 m has a georeferenced position in addition to another line position a significant distance away. Note that the 0.0 m position will not necessarily correspond to the "start" of any line in terms of its acquisition, but it will be near one end of the line (and there may be negative line positions).

Table 1. Georeferenced line positions and horizontal distances for each site (WGS 84, UTM Zone 20N).

Capacitively-Coupled Resistivity

Site	Line Position (m)	Easting (m)	Northing (m)	Distance (m)
01	0	378756	7339378	
01	300	378921	7339132	296.2
01x	0	378735	7339271	
01x	70	378774	7339337	76.7
02	0	379147	7339538	
02	500	379562	7339775	477.9
03	0	378902	7339062	
03	400	379182	7339341	395.3
04	0	379294	7339683	
04	422	379512	7339365	385.5
05	0	377409	7338728	
05	300	377674	7338860	296.1
06	0	377925	7338656	
06	250	378018	7338425	249.0
07	0	377860	7338673	
07	225	377798	7338459	222.8
08	0	377305	7338977	
08	140	377283	7338840	138.8
09	0	379163	7339606	
09	825	379856	7340047	821.4
10	0	378917	7339053	
10	120	378921	7338933	120.1
11	0	379518	7339847	
11	225	379624	7339647	226.4
12	0	378234	7338741	
12	650	378858	7338615	636.6

Galvanic Resistivity

Site	Line Position (m)	Easting (m)	Northing (m)	Distance (m)
01	0	378736	7339397	
01	357	378914	7339094	351.4
01x	0	378741	7339281	
01x	94	378783	7339366	94.8
015	0	378735	7339399	
015	235	378854	7339196	235.3
08	0	377298	7338923	
08	94	377280	7338833	91.8
11	0	379520	7339835	
11	357	379685	7339518	357.4

Since our surveys often follow geographic features such as rivers or roads, it is not always possible to orient lines positive in the East and North directions. In Pangnirtung, we orient lines positive in the general South-East (up-slope) and North-East (up-fjord) directions. Reference

points on each line are then used in conjunction with a digital elevation model to extract topographic profiles at 5 m intervals. Note that line positions are "along-the-ground" positions such that the horizontal distance between points may not be equal to the line distance. There is also some error in location of the reference points on each line. Differential GPS was used to locate line markers using the Canadian CDGPS correction service. However, GPS positions were noted to be very erratic. These location errors result in some misplacement of each topographic profile; the misplacement is distributed evenly along each line. Actual location errors are impossible to estimate, but synthetic inversions suggest that the effect on the electrical images is likely less detrimental than neglecting the topography. Table 1 shows the processed line locations. Note that the CCR and GR lines are not exactly aligned at each site. The distance between the zero positions can be found from the georeferenced coordinates.

After elimination of outliers and assignment of geometry, we can begin the inversion process. The measurements of current and voltage are not directly indicative of the subsurface material properties, but are related by the physics of the experiment. Inversion is the process of attempting to construct a model of material properties that adequately honours the observed data (e.g., Oldenburg and Li, 2005). In this case, the material property of interest is the electrical conductivity or its inverse, the electrical resistivity. The governing physics are those of the diffusion equation with a point source, and the inversion methodology is smoothness-constrained least-squares.

Capacitively-Coupled Resistivity

The inversion algorithm Res2DInv is that of Loke and Barker (1996) and Loke et al. (2003). The default CCR inversion parameters consist of an L_2 norm on the data and model, a horizontal to vertical flatness ratio of 0.3, global model regularization without a reference model, and a cooled regularization parameter from 0.2-0.04. Measurements are output from the OhmMapper as apparent resistivity (see below). Logarithmic transformations are used on both the data and the model. No bounds are placed on the recovered model values. The inverse model uses a constant cell size of 1.25 m in height and 2.5m in width.

The default inversion parameters are consistent for all CCR data sets. However, site-based noise levels and other factors make custom processing necessary, especially with regards to assessing convergence of the inversion. The level of convergence of the inversion is directly related to the level of noise in the data. Inversions of noisy data may converge after only a few iterations and the predicted misfit on the data may be quite high. Unfortunately, assessing the noise level associated with OhmMapper data can be difficult. Firstly, reciprocal measurements can never be repeated with control. Data are collected in a time-based manner with the transformation to spatial coordinates done via averaging betweens user-specified marks. The spatially transformed data are then sampled (via median selection) to a user-specified increment of 2.5 m in this case. There is unknown error inherent to both the spatial transformation and the sampling. Furthermore, there is model error associated with CCR data. The low induction number assumption and a geometric calibration are used to convert CCR measurements to apparent resistivity as if they were direct-current galvanic data (Kuras et al., 2006; Groom, 2008). We then employ the physics of DC potential fields with point sources for inversion. However, the OhmMapper is actually a low-frequency electromagnetic instrument with line

antennas. Equivalency to DC data is never exact and worsens for the cases of small dipole separations, high conductivity, or large dipoles.

Lacking a good quantitative method for estimating noise levels on capacitive resistivity data, we utilize the convergence behaviour of the inversion algorithm. In general, the capacitive data tend to converge to an RMS misfit level of approximately 20% after removal of obvious outliers; we will consider this to be the practical noise level. However, for data collected within the hamlet, convergence is slow, sometimes oscillatory, and can be as poor as 70%. The following protocol was adopted: given an RMS misfit in excess of 20%, an inversion is performed with iterative re-weighting of the data with a threshold of 10% misfit (often termed an L_1 norm on the data). The data are them trimmed to retain only the data with a misfit below the RMS misfit level at convergence of the L_1 inversion. This trimmed data set is then inverted with default parameters resulting in RMS misfits below 20%. However, we must remember that these inversions have been biased towards the inverse model.

Galvanic Resistivity

The same inversion software is used for the GR data as for the CCR data. The default GR inversion parameters consist of an L_2 norm on the data and model, a horizontal to vertical flatness ratio of 0.3, global model regularization without a reference model, and a cooled regularization parameter from 0.1-0.02. Measurements are transfer resistances in V/A; Res2DInv converts measured resistance data to apparent resistivity. Logarithmic transformations are used on both the data and the model. No bounds are placed on the recovered model values. The inverse model uses a constant cell size of one-half the electrode spacing in height and one electrode spacing in width.

GR data are less noisy than CCR data; the required regularization parameters are lower and the resulting models have a better fit. Furthermore, the collection of reciprocal measurements allows us to quantify the experimental error in the data (in this case, less than 1%). Convergence levels of 4-5% indicate that we have some additional systematic error in the inversion that we will not attempt to identify (e.g., Oldenborger et al., 2005).

RESULTS

The survey results are grouped into three main geographical areas with similar geophysical characteristics: the Alluvial Area, the Phase 2 Area, and the West-Hamlet Area (Figure 3). The areas correspond generally to the geomorphic domains indentified by Carbonneau and Allard (2009) and LeBlanc et al. (2010). These areas will be discussed in turn and for each survey line.

Models are presented for each line in terms of resistivity in Ωm. CCR and GR models are not exactly aligned; where appropriate, the positions of the zero marks for the GR models have been indicated on the CCR models. The colour scales are not the same for every image, but are the same or similar for each geographical area. Reds are resistive and generally interpreted as ice-rich and/or dry, coarse and porous sand/gravel. Blues are conductive and generally interpreted as wet and/or silt/clay-rich marine sediments or diamicton. Figure 2 illustrates the temperature-

conductivity relationship for different material types. The presence of high-salinity unfrozen water will cause any material type to appear conductive (e.g., Ross et al., 2007). To asses model quality, we compare the measured data to the data calculated for the inverse model. This is done on a spatial basis using measured and calculated apparent resistivity pseudosections for each line, in addition to reporting the global RMS measure of misfit. Limited uncertainty analysis has been performed to date, but depth of investigation computations (Oldenburg and Li, 1999; Oldenborger et al., 2007) have been performed on some models.

Alluvial Area

Line 01 and 01x, River

The Line 01 model is shown in Figure 7 for the CCR data and Figure 8 for the GR data. Comparing the different data types, we see that capacitive model values are generally more conductive (less resistive) than the galvanic model values. Galvanic results are more "trustworthy" in terms of material property values due to the lower noise, better fit to the data, and a more accurate representation of the experimental physics by the inversion. However, we do not have galvanic data at all locations. Henceforth, any material property values will be given the designation "GR" or "CCR" to indicate their origin and to facilitate comparison.

The conductive layer at the surface (left and right) corresponds to zones of standing water on the surface and is likely the signature of the active layer (~1000 Ωm GR, ~500 Ωm CCR) that extends to 2–3 m depth. The middle layer of extremely high resistivity is either very dry-porous gravel or very ice-rich or both (>60 kΩm GR, >30 kΩm CCR). The interpretation of a thick alluvial sheet is consistent with observable surface boulders and drilling results near the bridge (Hsieh and Tchekhovski, 2008). Estimates of thickness are unreliable due to the very high resistivity; highly restive layers can be imaged as thicker than reality in inverse models (e.g., Ingeman-Nielsen, 2005). However, the observation of variable thickness is likely sound with the unit thickening towards the fjord. Interesting to note is where the resistive layer "outcrops" in the middle of the section, which could be followed up with georadar or shallow drilling observations. The crossline models illustrated in Figure 9 for the CCR data and Figure 10 for the GR data suggest that this layer also outcrops near the housing structures adjacent (NE) to the river (Figure 6), but is significantly less resistive near the surface. There seems to be significant 3D heterogeneity to the shallow subsurface as evidenced by the crossline model.

There is an indication of more conductive material at depth (~5 kΩm GR, ~2 kΩm CCR) on the up-river part of the section and on the crosslines away from the river – these are the directions in which we might expect thinning of an alluvial sheet. Borehole information indicates a stable subsurface temperature of approximately -3°C at depth. At this temperature, a resistivity of 1000 Ωm corresponds approximately to frozen sand or silt (Figure 2) or perhaps marine sediments with low moisture content, but high salinity. The observed resistivity of the lower layer does not correspond to that of the till observed in the Phase 2 data (discussed below).

Line 10, Reservoir-River Road

The Line 10 model is shown in Figure 11 for CCR data only. This section is an extension (with gap) of Line 01, but there is a significant change in direction. We observe the same conductive over resistive over conductive pattern as in Line 01 with similar CCR property values. There is no obvious change in the subsurface as we approach the modern river channel. However, coverage is poor at the end of the section.

Line 03, Reservoir Road

The Line 03 model is shown in Figure 12 for CCR data only. This model is along the base of the current reservoir. It is noisy due to several culverts and drainage paths passing under the road (evident as the near-surface resistive circular features). The model indicates a transition from a highly resistive subsurface (interpreted as sand/gravel) to a layered model (described below in the context of the Phase 2 Area). Comparing Figures 7, 9 and 11 to Figure 12, there is a significant difference in character between the other models in the Alluvial Area and along the reservoir road. Line 03 corresponds to the transition on surface between alluvial fan and till as mapped by Carbonneau and Allard (2009). However, the resistivity model suggests a resistive surface layer (~3 kΩm CCR) overtop of the till (~50 Ωm CCR). The resistive surface layer may be attributed to roadbed material, or colluvial material that extends higher upslope than that mapped by Carbonneau and Allard (2009).

Line 12, Arena Road

The Line 12 model is shown in Figure 13 for CCR data only. This model is a continuation of the Line 03 model on the other side of the river. Collected within the hamlet, this data set is very noisy and many data points had to be removed. The modelling also contains errors because the true survey path along the road deviates significantly from a straight line. Nevertheless, the model shows a clear transition from the alluvial fan to more conductive, but complicated, material differing from the Phase 2 type of layered model. The Line 12 model shows little evidence of layering either in the Hamlet or on the alluvial fan. However, there does seem to be a finite thickness to the fan, and there does seem to be some overlapping of conductive material onto the western shoulder of the fan. The circular resistive feature at approximately 90 m is likely the culvert passing under the road beside the arena – its exact position is hard to verify because of the non-linear nature of the section.

Phase 2 Area

Line 11, Phase 2 BH

The Line 11 model is shown in Figure 14 for the CCR data and Figure 15 for the GR data. This model is typical of the Phase 2 Area which seems to be a 2-layer model with limited slope-scale heterogeneity. The resistive surface layer (~6 kΩm GR, ~3 kΩm CCR) is interpreted as frozen sand/silt 2–3 m thick. When interpreting depths, capacitive data are noisier, but have higher near-surface resolution and provide a better depth estimate. Furthermore, resistive layers tend to appear thicker than reality in inverse models (e.g., Ingeman-Nielsen, 2005). At the scale

of the survey, the active layer thickness of ~1 m cannot be resolved. Observed small-scale heterogeneity is interpreted to be a result of more ice-rich zones, particularly near SDH-20. Further upslope near the end of the section, increased resistivity may be related to high boulder occurrence which would also increase the resistance.

The underlying layer is conductive (~200 Ωm GR, ~100 Ωm CCR). At the recorded temperature of -7°C at 10 m depth, these resistivities correspond to clay/clay-till. There seems to be increased conductivity towards the fiord at depth which may be related to the landfill and vehicle graveyard at the foot of the slope, or to seawater intrusion. Again, the model based on the CCR data is significantly more conductive, but the general features are the same including the location of higher resistivity zones at the surface. The resistivity models corroborate the Phase 2 Area mapping of colluvial material overlying till (Carbonneau and Allard, 2009). However, based on the electrical properties, we posit that the till is likely clay-rich or has high porewater salinity (e.g., Hyatt, 1992).

Line 04, Phase 2

The Line 04 model is shown in Figure 16 for CCR data only. This model suggests an increase in conductivity of the lower layer (~50 Ωm CCR) in the western zone of Phase 2 as seen in Line 03. Changes across-slope from Line 11 include increased variability in the lower layer in both the up- and down-slope zones. The increased incidence of boulders is also evident in the up-slope portion of the model.

Line 02, Phase 2

The Line 02 model is shown in Figure 17 for CCR data only. This model joins Line 04 and Line 11 and further illustrates the relative across-slope homogeneity of the Phase 2 Area. Apparent from this section is the increase in resistivity of the underlying layer from the southwest (Line 4) to the northeast (Line 11) ends of the section. The small conductive feature at the very southwest end of the section is suspect, but corresponds to the location of the engineered roadbed.

Line 09, Sewage Road

The Line 09 model is shown in Figure 18 for CCR data only. This model runs along the road passing by the sewage treatment plant and the landfill. The data are noisy, presumably due to cultural interference of the buildings and the road/ditch. Signal loss was a serious issue for this line and thus, model depth is limited compared to the other Phase 2 data. Consistent with signal loss is a lower surface resistivity compared to the other Phase 2 data. This may be a result of the roadbed engineering and materials, moisture retained under the road, or perturbation of the thermal profile by the road. The presence of more conductive shallow material from approximately 330–610 m is correlated to the location of the landfill and vehicle graveyard along the road.

West-Hamlet Area

Line 08, Park

The Line 08 model is shown in Figure 19 for the CCR data and Figure 20 for the GR data. The park model exhibits a dipping contact between a resistive surface layer (variable, >10 kΩm GR and CCR) that extends to approximately 4 m depth, and a conductive lower layer (~500 Ωm GR and CCR). The GR data are not as noisy as the CCR data and result in a much cleaner model. However, the coverage associated with the deployment of a single Wenner array is limited in horizontal extent.

The area is mapped as colluvium over silty marine sediments (Carbonneau and Allard, 2009) and SDH-10 intersects a contact between sand and silt at ~2.2m depth. This is in good agreement with the location of the contact that can be inferred from Figure 19 and the electrical model can be used to extend the contact northward. Based on the observed resistivities, the surface colluvium appears to be discontinuous or variable. The regions of particularly high resistivity may be associated with ice-rich sands. The resistivity of the underlying material is higher than expected for marine sediments with presumably high salt content, and is actually higher than that of the underlying till in the Phase 2 Area (500 Ωm vs. 50–100 Ωm CCR).

Also noteworthy is that bedrock outcrops at the surface within metres of the section to the north, and was encountered at 6 m depth during construction to the south of the section. Unless highly fractured with unfrozen saline porewater, bedrock should represent a resistive anomaly. We can indentify no such anomaly in the resistivity models, which suggests extreme variability of the bedrock surface.

Line 05, Runway

The Line 05 model is shown in Figure 21 for CCR data only. This model shows similar structure to Line 08. However, the underlying material is more conductive (~50 Ωm CCR) and there is a high resistivity anomaly approximately 80 m in width that extends to depth. In light of the variable bedrock surface, this anomaly could be interpreted to be a bedrock high. However, no outcrop was observed during data acquisition. Alternatively, the anomaly may be interpreted to be an ice-rich region extending into the underlying material. The recovered resistivity is relatively low for either bedrock or ice. However, based on GR results, the true resistivity may be much higher than that modelled in Figure 21. Unfortunately, the Line 05 data are contaminated by a large degree of cultural noise, with airport fencing to the south and houses with heating oil tanks to the north, making confident interpretation difficult.

Line 06, Tower

The Line 06 model is shown in Figure 22 for CCR data only. We see a structure similar to that observed on the Phase 2 slopes: a resistive surface layer (~2 kΩm CCR) with more conductive underlying material (~50 Ωm CCR). The model is consistent with the mapping of colluvium over till (Carbonneau and Allard, 2009). However, surface resistivities are not as high as in the Phase 2 Area suggesting some difference in the colluvial material. Furthermore, the

thickness of the colluvial material exhibits more spatial variability. Upslope, the thickening high resistivity feature is consistent with the edge of the moraine that has been reported to be ice-cored. The high resistivity could also be a result of a high incidence of boulders. The conductive down-slope anomaly is likely a combination of noise associated with the radio tower and the crossing of a small creek.

Line 07, SDH-05

The Line 07 model is shown in Figure 23 for CCR data only. This model is a lower elevation complement to Line 06. The up-slope resistive anomaly is not observed on Line 07 (which is at a lower elevation), but all other interpretations remain essentially the same.

CONCLUDING DISCUSSION

Two-dimensional (2D) electrical geophysical data have proven useful for aiding geomorphologic mapping of permafrost conditions in Pangnirtung, Nunavut. The geophysical data provide subsurface information to extend the results of shallow borehole drilling both horizontally and vertically. In most cases, we can identify mapped surficial sediments in the geophysical models in addition to providing information on underlying materials. The shallow boreholes provide information at a much higher vertical resolution than the geophysical data such that direct correlation of features observed in the boreholes at sub-meter scales is not possible. Furthermore, most of the completed boreholes did not reach reached depths greater than 3 m such that ground-truthing of the electrical models at depth is not possible.

Nevertheless, we are able to confirm the observed heterogeneity of material types across the hamlet of Pangnirtung. The electrical models reveal distinct zones of material properties that correspond well to mapped sedimentary units. Furthermore, we are able to assign approximate electrical properties to many of the units, in addition to adding some information on variability within each of the units, including the identification of potentially ice-rich zones. The Area-based ranges of electrical properties presented below attempt to encompass some of the observed spatially variability, and the discrepancy between CCR and GR models (where GR data exist).

The Alluvial Area exhibits significant variability in the subsurface. The simplified electrical model consists of three layers with a conductive surface layer (500–1000 Ωm) over a resistive middle layer (>30 kΩm) over underlying conductive material (2–5 kΩm). The surface layer in interpreted to be the active layer with high unfrozen water content. It is not continuous across the area and its thickness is variable. The middle layer corresponds to the mapped unit of alluvial sand, gravel and boulders. It is interpreted to increase in thickness both down-river and toward the river perpendicular to the flow direction. Based on comparison to other data, the underlying layer is interpreted to be similar to the material identified in the West-Hamlet Area as silty marine sediments, however there is significant uncertainty.

The Phase 2 Area appears relatively homogeneous. The simplified electrical model is a two-layer model with a resistive surface layer (3–6 kΩm) over underlying conductive material (100–200 Ωm). These layers are interpreted to correspond to the mapped units of colluvium and till

respectively. Small-scale regions of high resistivity are observed in the colluvium which are interpreted to be regions of high ice or boulder content. The electrical data suggest that the till is clay-rich or has high porewater salinity.

Interpretation of models in the West-Hamlet Area is hampered by poor data quality resulting from cultural noise. The simplified electrical model is a two-layer model with a resistive surface layer (>10 kΩm) over underlying conductive material (50–1000 Ωm). The surface layer is well-correlated with the sandy colluvial material observed in a shallow borehole and mapped across the region. The underlying material corresponds to silty marine sediments, also observed in the shallow borehole. Both the surface and underlying material appear variable in both spatial extent and material properties. This may be a result of variation in ice content or salinity, or it may be an artefact of the large degree of cultural noise. The southern slopes of the West-Hamlet Area are more similar in electrical characteristics to the Phase 2 Area. This observation is corroborated by the surficial mapping. However, lower observed resistivity suggests that the colluvial material in the West-Hamlet Area has a somewhat higher fine content, a lower ice content, or more unfrozen water.

It should be cautioned that limited uncertainty analysis has been carried out on the electrical models. Features near boundaries of the electrical models are suspect. Moreover, with very resistive subsurface features, estimating material properties and layer depth/thickness is subject to a high degree of nonuniqueness. In such cases, direct correlation with boreholes or synthetic modelling may be the only reliable ways of estimating resistivity and layer thickness. When comparing the GR and CCR data types, it should be noted that the GR data have lower noise, converge to better RMS misfits and likely represent more accurate estimates of the true material properties. However, the CCR data are collected at a much higher spatial interval and with smaller dipole separations, such that the near-surface resolution is superior. It follows that the CCR models likely provide better estimates of depth and spatial extent of model features. Future work will involve synthetic modelling to better constrain model depths, uncertainty analysis, and more detailed integration of the electrical models with georadar data and deep borehole records.

ACKNOWLEDGMENTS

This work was conducted under the Climate Change Program of Natural Resources Canada with funding provided by the Canada Nunavut Geoscience Office and in cooperation with the Centre d'études nordiques at Université Laval, the Government of Nunavut, and the hamlet of Pangnirtung. Field data were collected with assistance from W. Sladen, J. Uniushagak, P. Gosselin, and A.-S. Carbonneau. Data and models are available from the author. Project logistics were handled by A.-M. Leblanc, D. Mate, and R. Mongeau. Satellite imagery was provided by the Government of Nunavut. Aerial images of Pangnirtung and line location overlays were provided by E. L'Herault. DEM data were provided by P. Gosselin, A.-S. Carbonneau, and E. L'Herault. Constructive review and editing was provided by N. Couture.

REFERENCES

Carbonneau, A.-S., and Allard, M., 2009. Assessing permafrost conditions and landscape hazards in support of climate change adaptation in Pangnirtung, Nunavut, in ArcticNet 6th Annual Scientific Meeting, Victoria.

Carbonneau, A.-S., Gosselin, P., L'Herault, E., Allard, M., Oldenborger, G., Leblanc, A., Sladen, W., and Mate, D., 2009. Assessing permafrost conditions and landscape hazards in support of climate change adaptation in Pangnirtung, Nunavut, in ArcticNet 6th Annual Scientific Meeting, Victoria.

Groom, D., 2008. Common misconceptions about capacitively-coupled resistivity (CCR): What it is and how it works, in *Symposium on the Application of Geophysics to Environmental and Engineering Problems*, 1345-1350, Environmental and Engineering Geophysical Society.

Hoekstra, P., Sellmann, P. V., and Delaney, A., 1975. Ground and airborne resistivity surveys of permafrost near Fairbanks, Alaska, *Geophysics*, 40(4), 641-656.

Hsieh, E. T., and A. Tchekhovski, 2008. Geotechnical Investigation and Foundation Design Recommendation, New River Bridge, Pangnirtung, Nunavut, AMEC Earth and Environmental.

Hyatt, J. A., 1992. Cavity development in ice-rich permafrost, Pangnirtung, Baffin Island, Northwest Territories, *Permafrost and Periglacial Processes*, 3, 293-313.

Ingeman-Nielsen, T., 2005. Geophysical Techniques Applied to Permafrost Investigations in Greenland, Ph.D., Technical University of Denmark.

Isherwood, A. E., 1983. New Pangnirtung Water Reservoir Detailed Geotechnical Investigation, Thurber Consultants Ltd.

Klein, K. A., and Santamarina, J. C., 2003. Electrical conductivity in soils: Underlying phenomena, *Journal of Environmental and Engineering Geophysics*, 8(4), 263-273.

Kuras, O., Beamish, D., Meldrum, P. I., and Ogilvy, R. D., 2006. Fundamentals of the capacitive resistivity technique, *Geophysics*, 71(3), G135-G152.

LeBlanc, A.-M., Oldenborger, G., Sladen, W., Mate, D., Carbonneau, A., Gosselin, P., L'Herault, E., and Allard, M., 2010. Assessing permafrost conditions in support of climate change adaptation in Pangnirtung, Nunavut, in Proceedings of the Sixth Canadian Conference on Permafrost, Calgary.

Loke, M. H., and Barker, R. D., 1996. Rapid least-squares inversion of apparent resistivity pseudosections by a quasi-Newton method, *Geophysical Prospecting*, 44(1), 131-152.

Loke, M. H., Acworth, I., and Dahlin, T., 2003. A comparison of smooth and blocky inversion methods in 2D electrical imaging surveys, Exploration Geophysics, v. 34, p. 182-187.

McNeil, J. D., 1980. Electrical conductivity of soils and rocks, Technical Note TN-5, Geonics.

Oldenburg, D., and Li, Y., 1999. Estimating depth of investigation in dc resistivity and IP surveys, *Geophysics*, 64(2), 403-416.

Oldenburg, D. W., and Li, Y., 2005. Inversion for applied geophysics: A tutorial, in *Near-Surface Geophysics*, edited by D. K. Butler, pp. 89-150, Society of Exploration Geophysicists.

Oldenborger, G. A., Routh, P. S., and Knoll, M. D., 2005. Sensitivity of electrical resistivity tomography data to electrode position errors, *Geophysical Journal International*, 163, 1-9.

Oldenborger, G. A., Routh, P. S., and Knoll, M. D., 2007. Model reliability for 3D electrical resistivity tomography: Application of the volume of investigation index to a time-lapse monitoring experiment, *Geophysics*, 72(4), F167-F175.

Pandit, B. I., and King, M. S., 1979. A study of the effects of pore-water salinity on some physical properties of sedimentary rocks at permafrost temperatures, *Canadian Journal of Earth Sciences*, 16, 1566-1580.

Pullan, S. E., Hunter, J. A., and Gilbert, R., 1983. A shallow seismic survey on the intertidal flats at Pangnirtung, Baffin Island, Northwest Territories, *Geological Survey of Canada Current Research*, 83-1B, 273-277.

Ross, N., Brabham, P. J., Harris, C., and Christiansen, H. H., 2007. Internal structure of open system pingos, Adventdalen, Svalbard: The use of resistivity tomography to assess ground-ice conditions, *Journal of Environmental and Engineering Geophysics*, 12(1), 113-126.

Scott, W. J., Sellmann, P. V., and Hunter, J. A., 1990. Geophysics in the study of permafrost, in *Geotechnical and Environmental Geophysics*, edited by W. J. Ward, 355-384, Society of Exploration Geophysicists.

Smith, L. B., Notenboom, W. G., Campbell, M., Cheema, S., and Smyth, T., 1989. Pangnirtung water reservoir: Geotechnical aspects, *Canadian Geotechnical Journal*, 26, 335-347.

Telford, W. M., Geldart, L. P., and Sheriff, R. E., 1990. Applied Geophysics, Second Edition, Cambridge University Press.

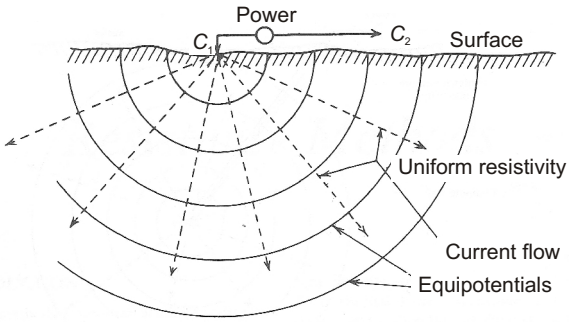

Figure 1. Current injection and resulting potential distribution for a point source (Telford et al., 1990).

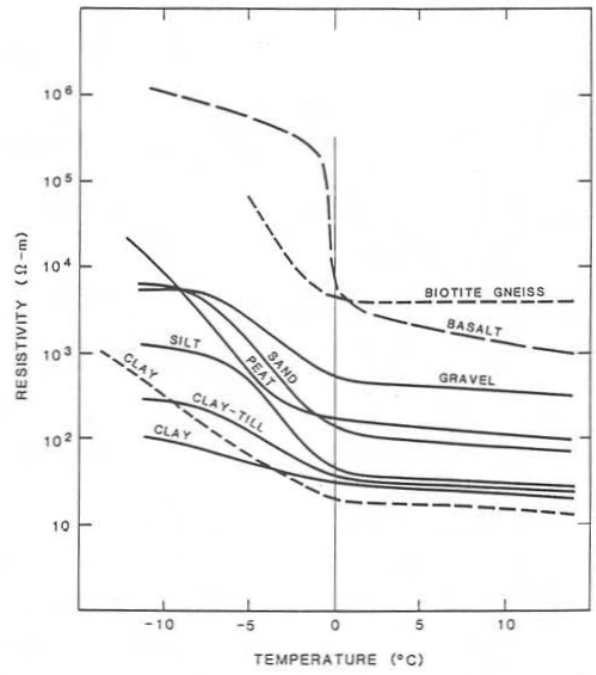

Figure 2. Variation in resistivity with temperature for different material types (Scott et al., 1990).

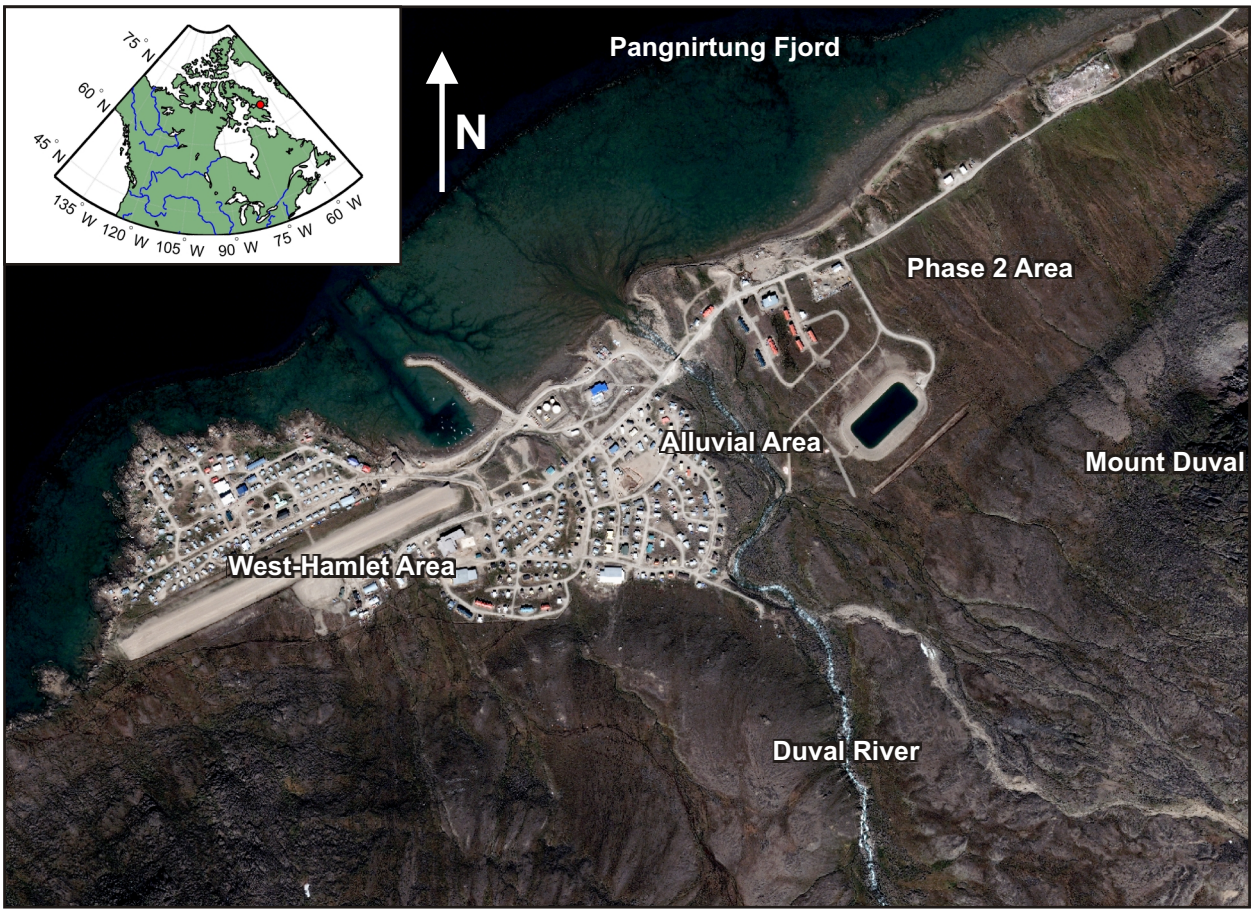

Figure 3. Aerial view of the hamlet of Pangnirtung, Nunavut with inset location map. Visible infrastructure includes the airport runway and the water reservoir. The geophysical data are discussed in terms of the illustrated general areas.

a)

b)

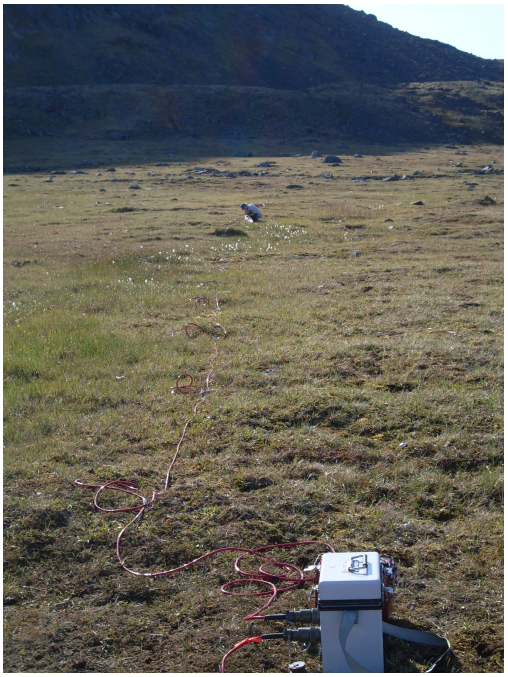

Figure 4. a) Capacitively-coupled resistivity system on Line 03. b) Galvanic resistivity system on Line 11.

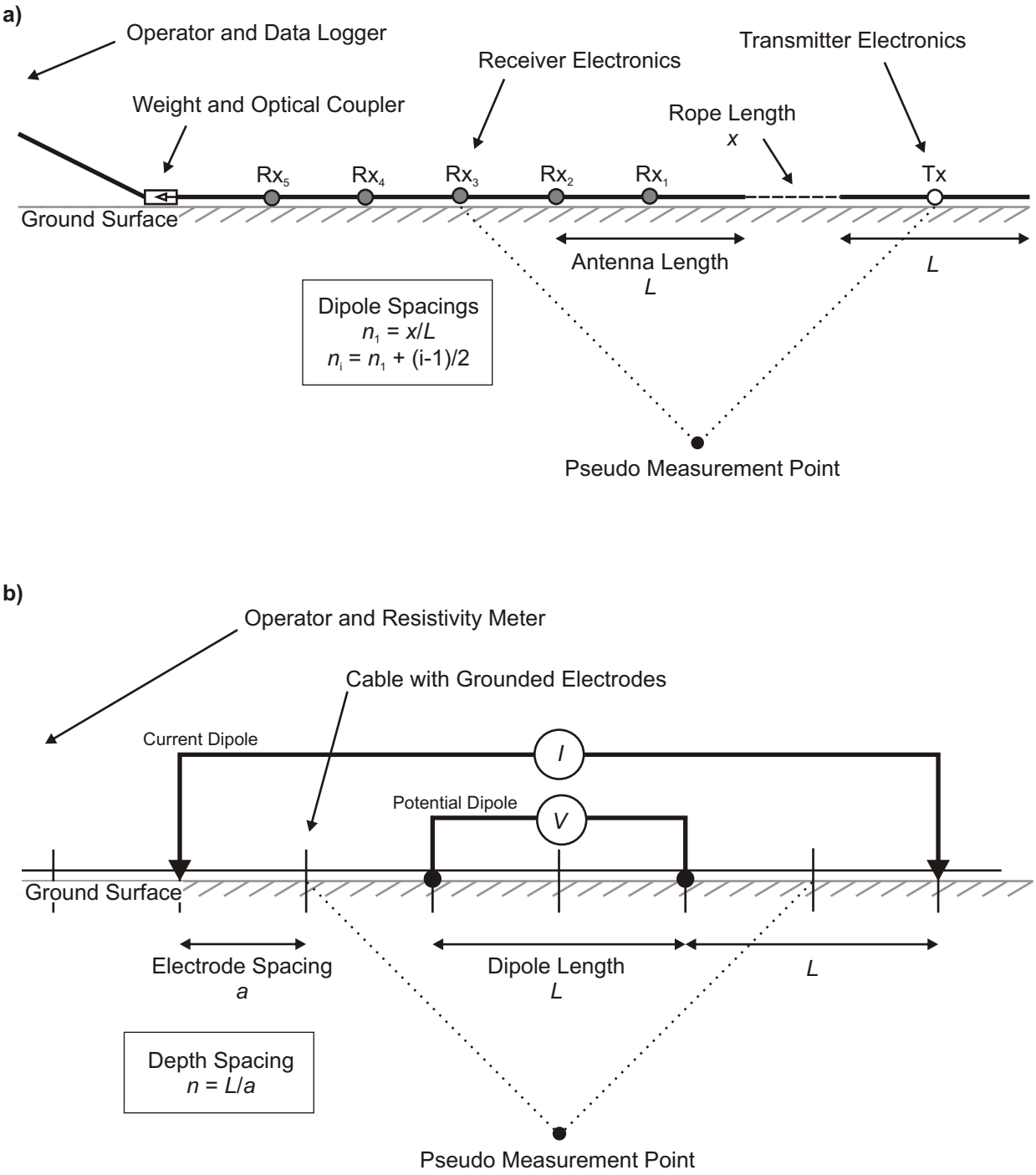

Figure 5. Schematic survey geometry. a) Capacitively-coupled resistivity: dipole-dipole array with 5 receivers. Note that adjacent receivers share one-half of an antenna. For a rope length of $x = L/2$, dipole spacings are $n = 0.5, 1.0, 1.5, 2.0, 2.5$ for receivers 1 through 5. The entire array is physically pulled along the ground surface. b) Galvanic resistivity: Wenner array. Reciprocal Wenner measurements involve a reversal of the current and potential electrodes. The measurement dipoles are moved along the electrode cable via electronic switching.

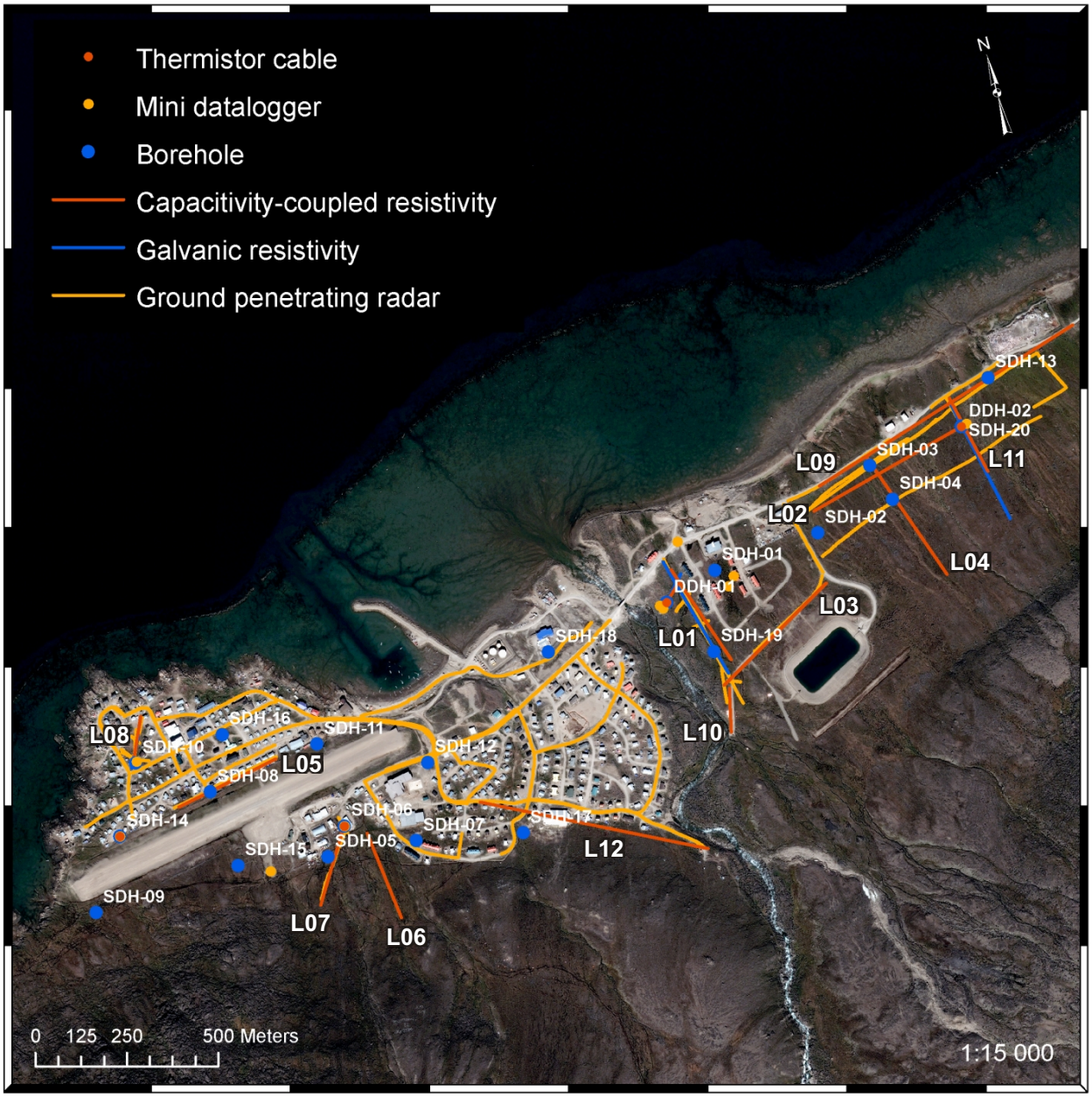

Figure 6. Location of CCR (orange) and GR (blue) sections in addition to georadar sections, shallow boreholes (SDH), deep boreholes (DDH), thermistors, and surface temperature data loggers. Electrical geophysical lines discussed in the text are identified as "L01" and so forth.

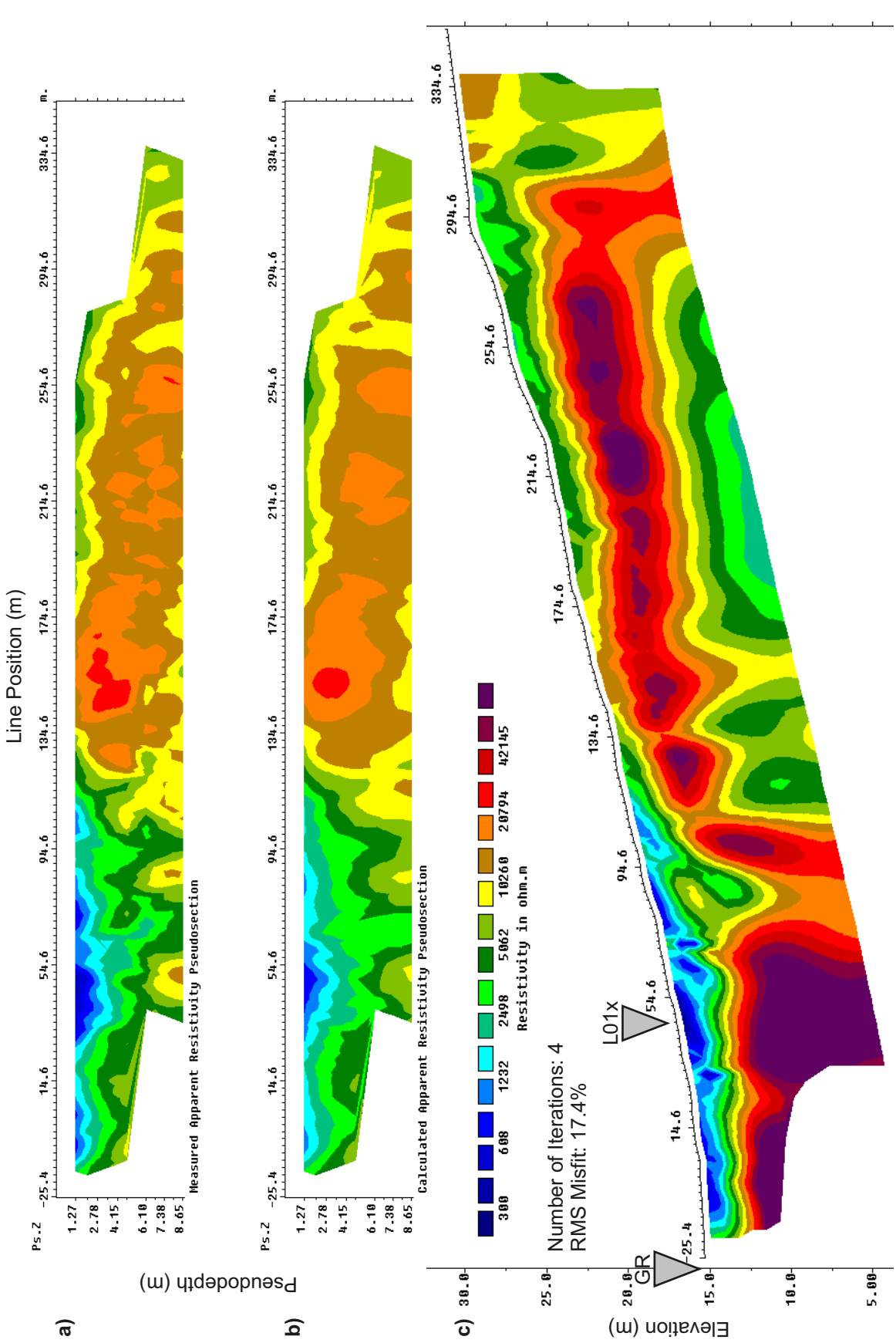

Figure 7. CCR model for Line 01. a) Measured apparent resistivity pseudosection. b) Calculated apparent resistivity pseudosection. c) Recovered resistivity model. Markers indicate the crossing position of Line 01x and the zero position of the corresponding GR model.

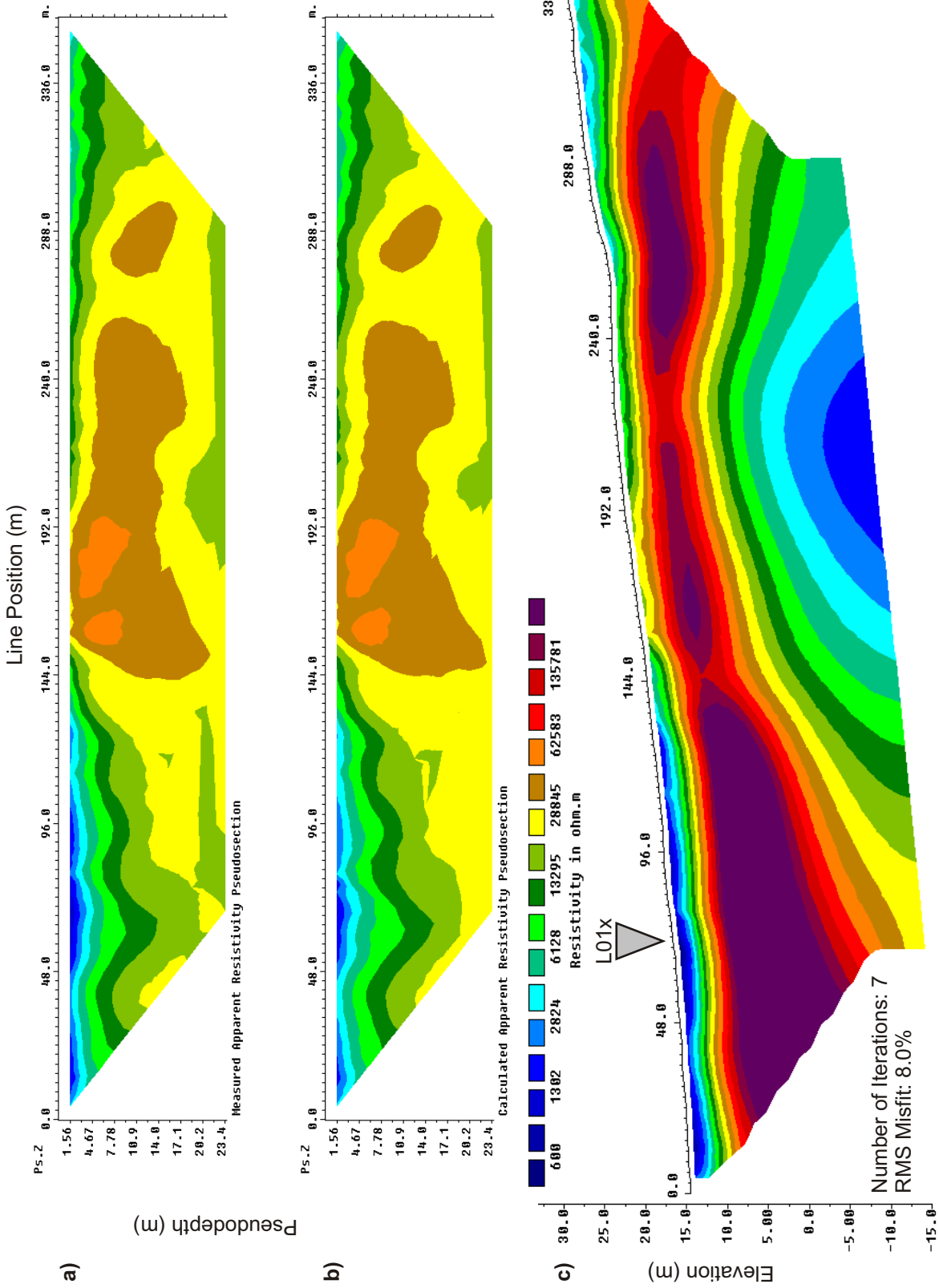

Figure 8. GR model for Line 01. a) Measured apparent resistivity pseudosection. b) Calculated apparent resistivity pseudosection. c) Recovered resistivity model. Marker indicates the crossing position of Line 01x.

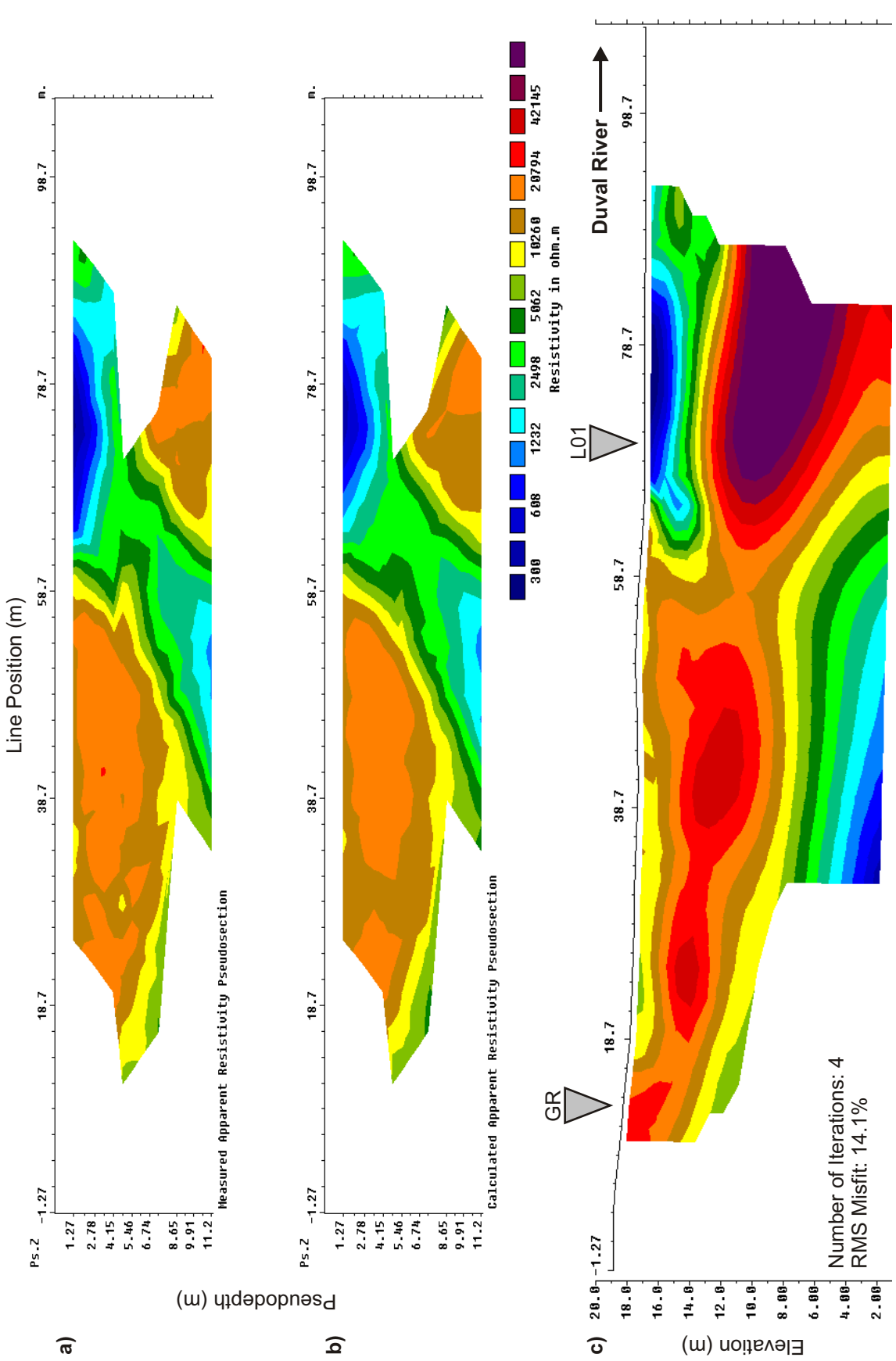

Figure 9. CCR model for Line 01x. a) Measured apparent resistivity pseudosection. b) Calculated apparent resistivity pseudosection. c) Recovered resistivity model. Markers indicate the crossing position of Line 01 and the zero position of the corresponding GR model.

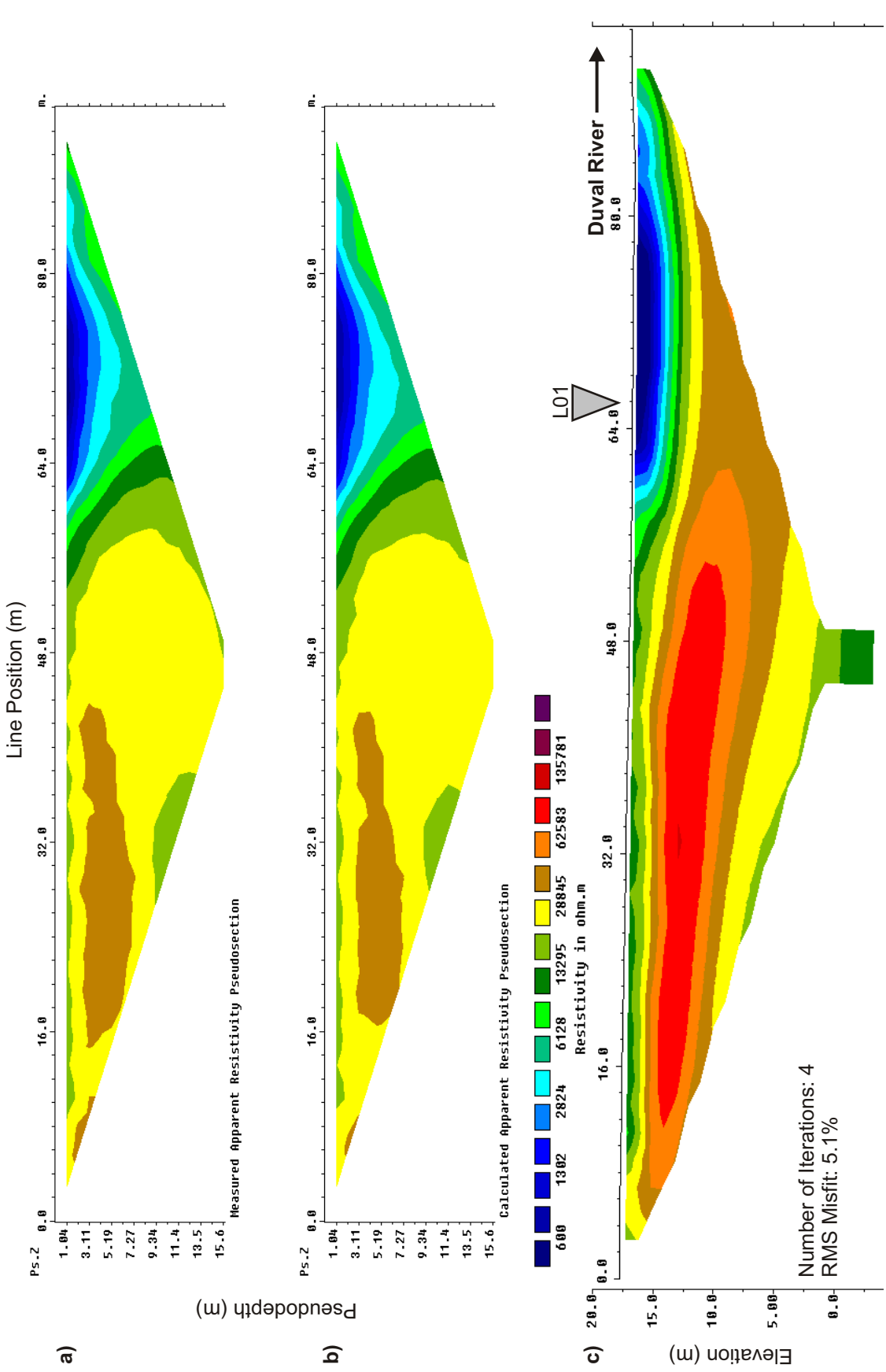

Figure 10. GR model for Line 01x. a) Measured apparent resistivity pseudosection. b) Calculated apparent resistivity pseudosection. c) Recovered resistivity model. Marker indicates the crossing position of Line 01.

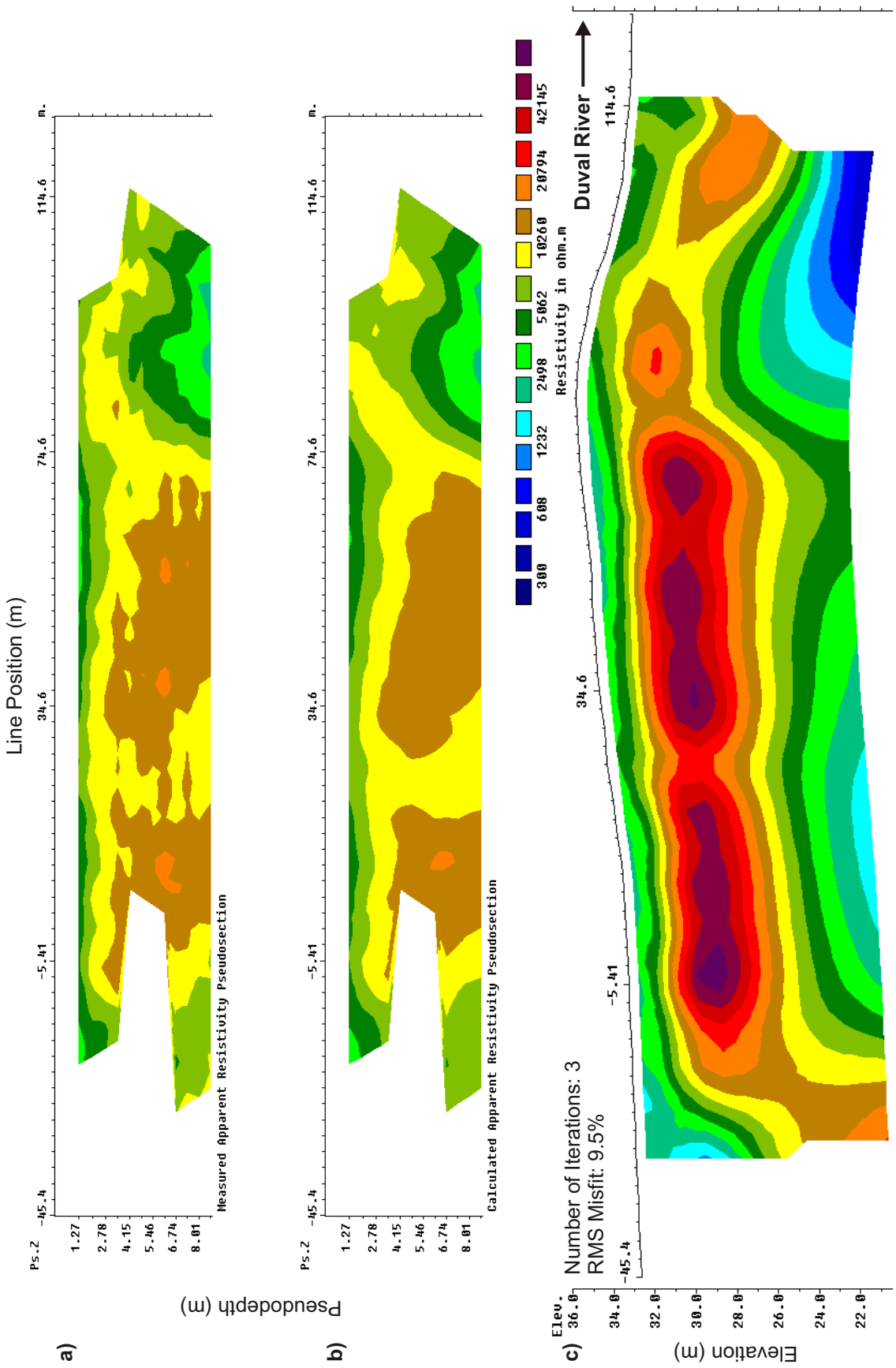

Figure 11. CCR model for Line 10. a) Measured apparent resistivity pseudosection. b) Calculated apparent resistivity pseudosection. c) Recovered resistivity model.

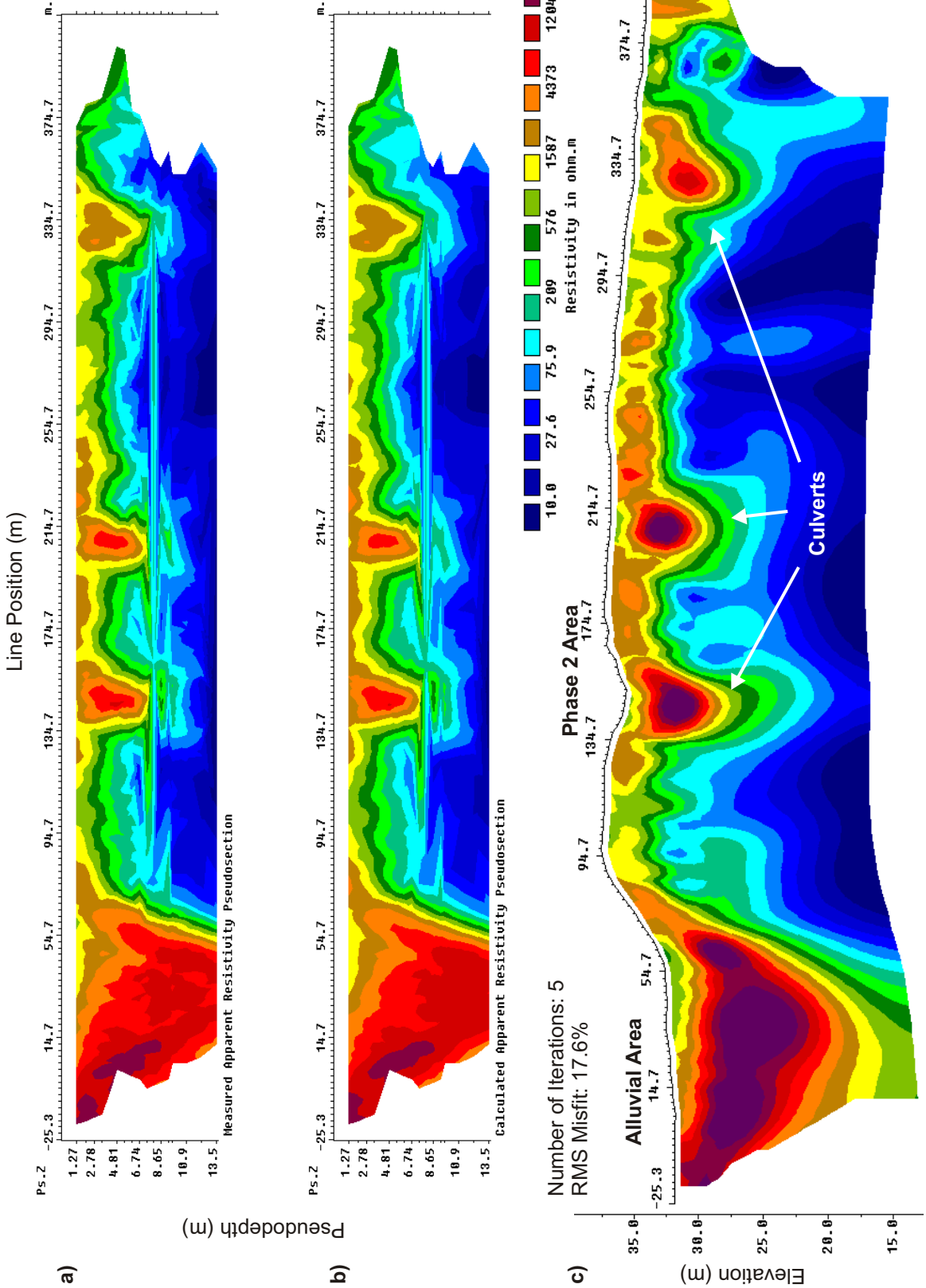

Figure 12. CCR model for Line 3. a) Measured apparent resistivity pseudosection. b) Calculated apparent resistivity pseudosection. c) Recovered resistivity model. The erratic appearance of the pseudosections is an artefact of the contouring procedure. The transition in terrain types occurs at approximately 95 m.

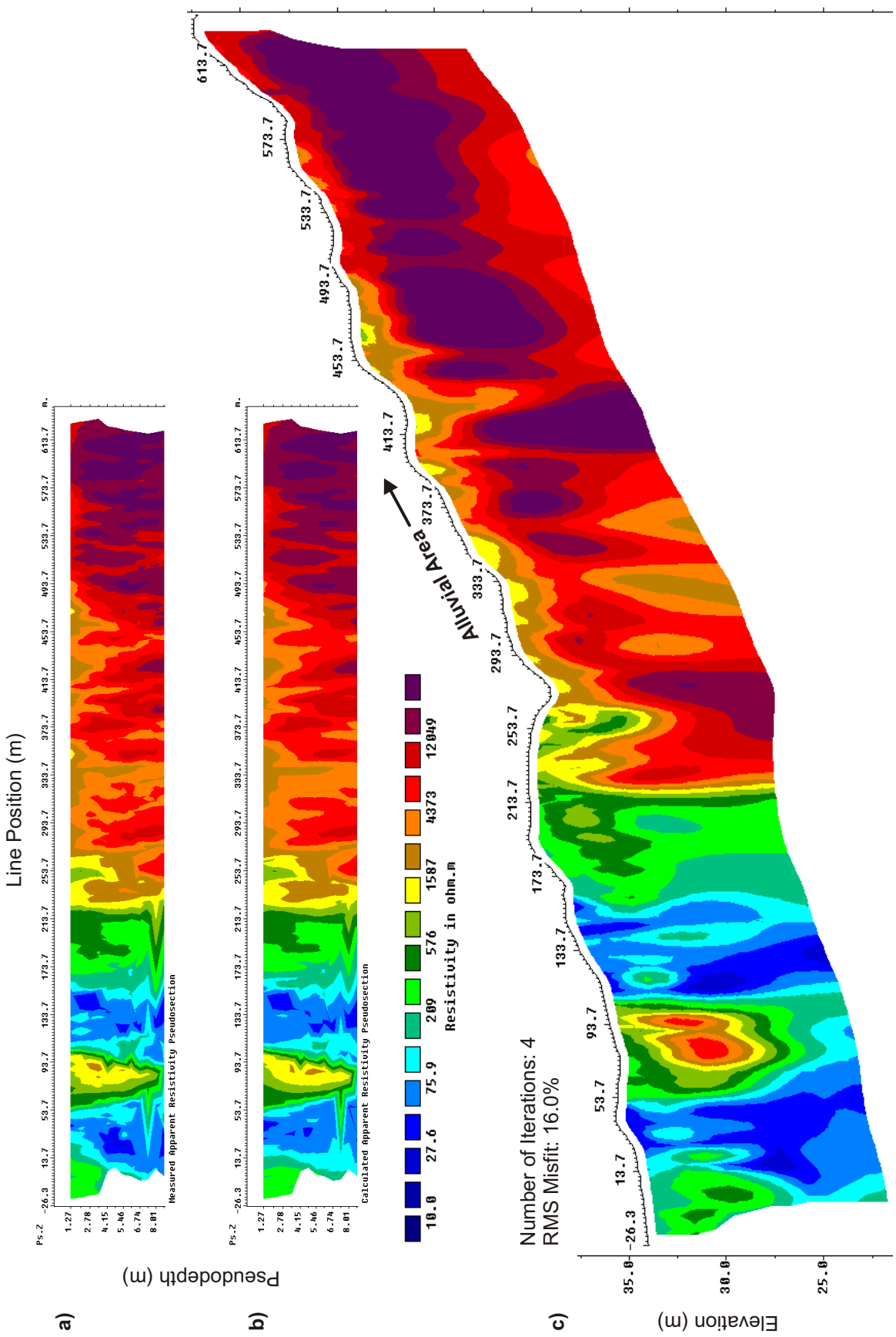

Figure 13. CCR model for Line 12. a) Measured apparent resistivity pseudosection. b) Calculated apparent resistivity pseudosection. c) Recovered resistivity model. The erratic appearance of the pseudosections is an artefact of the contouring procedure. The transition in terrain types occurs at approximately 215 m.

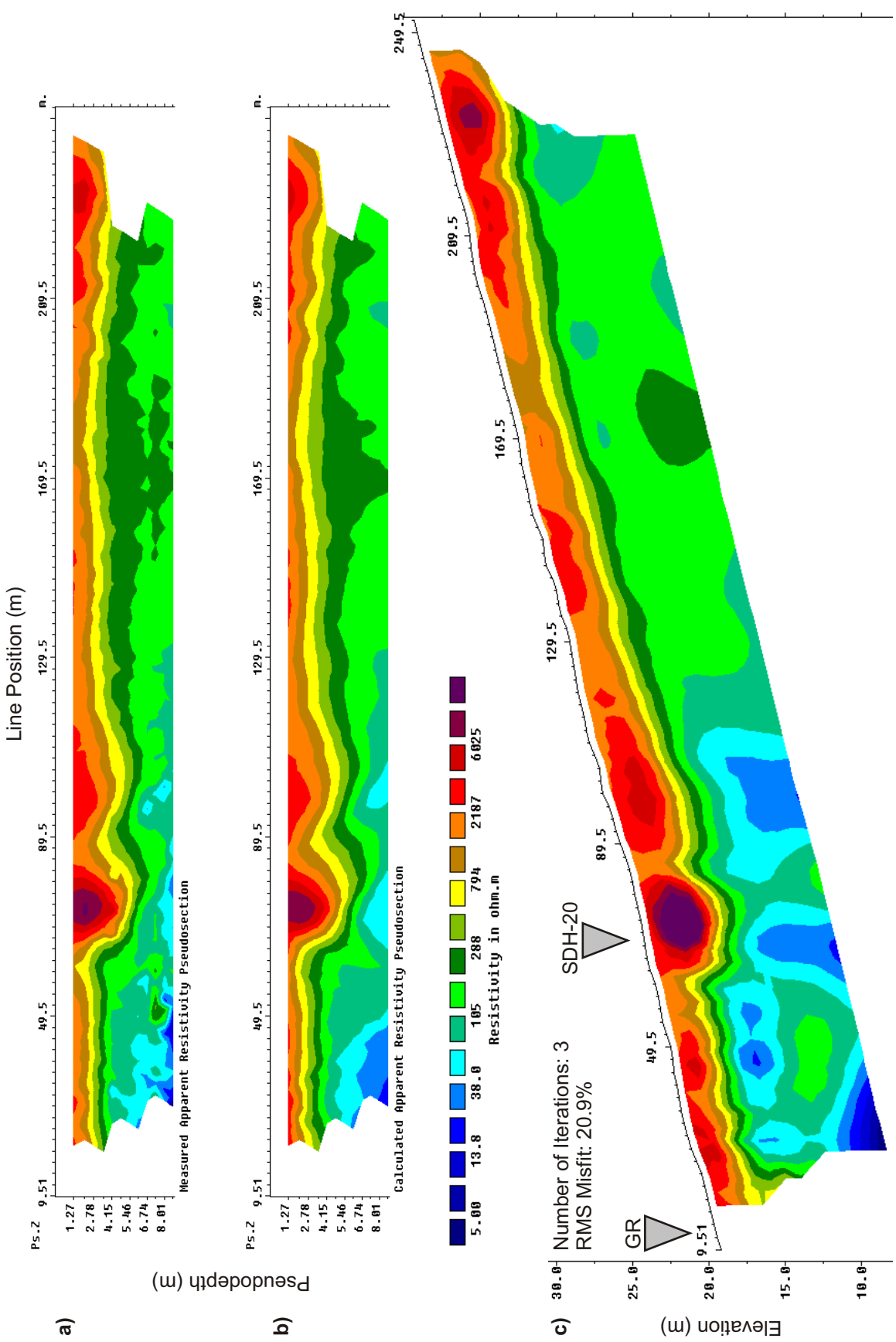

Figure 14. CCR model for Line 11. a) Measured apparent resistivity pseudosection. b) Calculated apparent resistivity pseudosection. c) Recovered resistivity model. Markers indicate the zero position of the corresponding GR model and the borehole location.

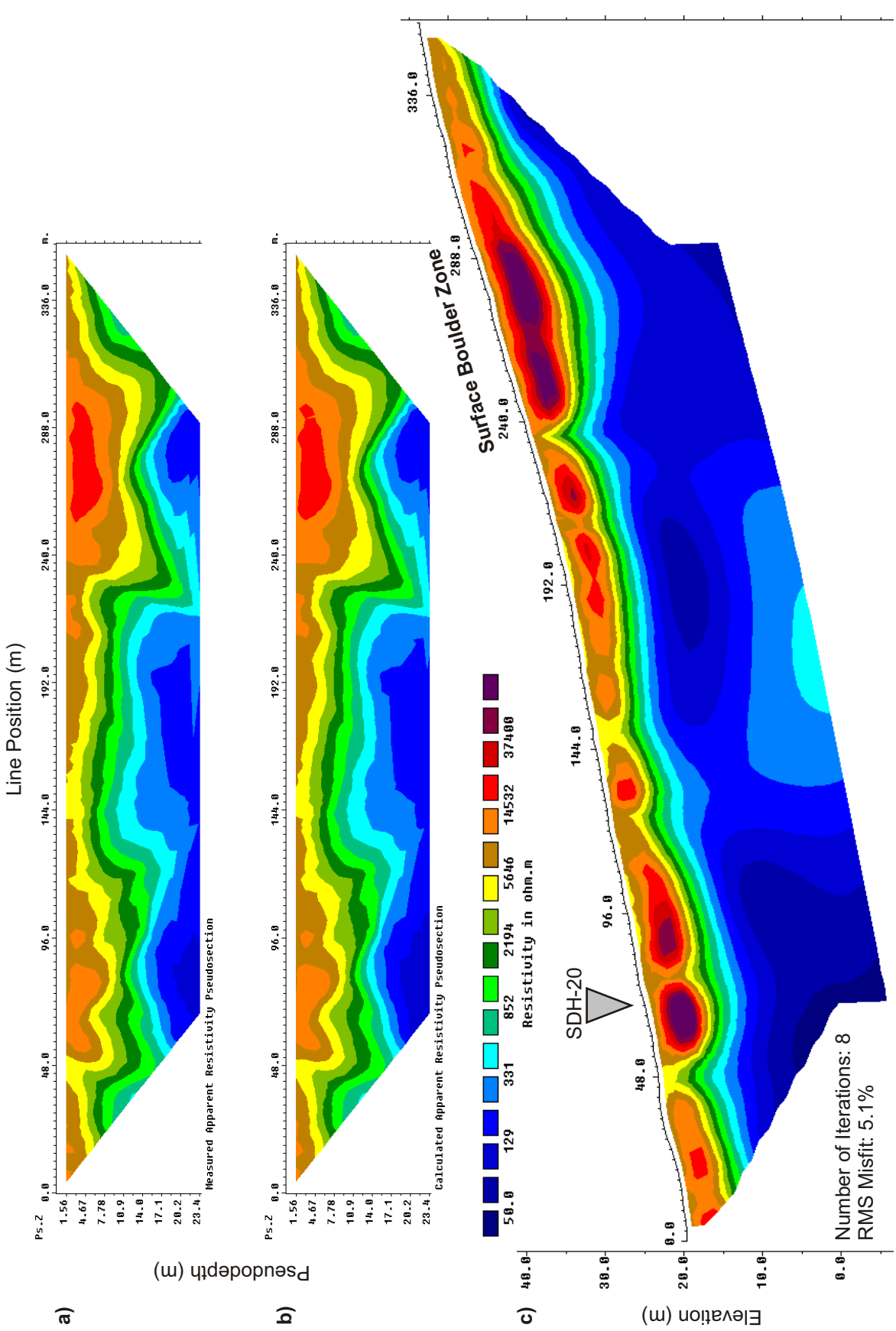

Figure 15. GR model for Line 11. a) Measured apparent resistivity pseudosection. b) Calculated apparent resistivity pseudosection. c) Recovered resistivity model. Marker indicates the borehole location.

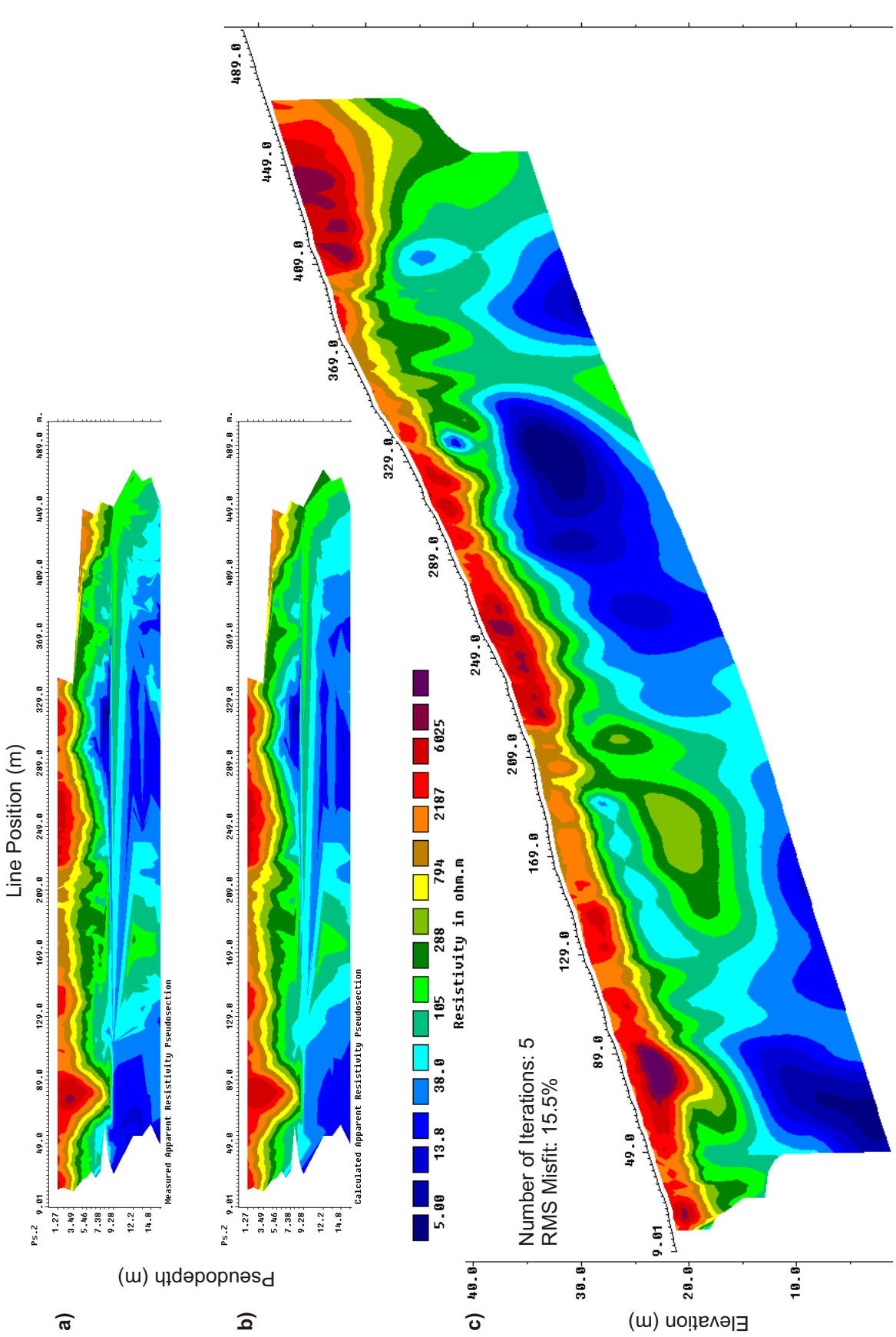

Figure 16. CCR model for Line 04. a) Measured apparent resistivity pseudosection. b) Calculated apparent resistivity pseudosection. c) Recovered resistivity model. The erratic appearance of the pseudosections is an artefact of the contouring procedure.

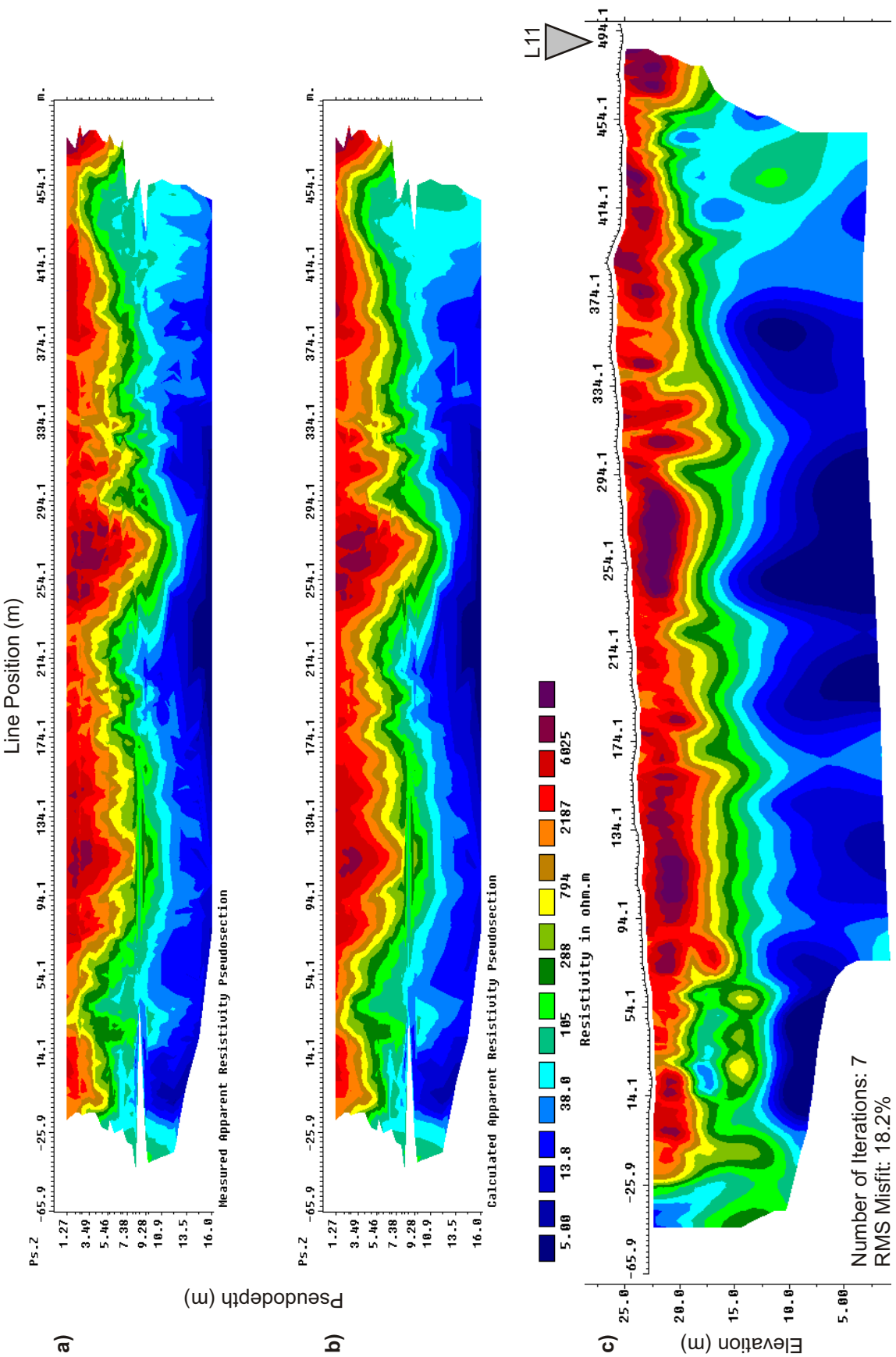

Figure 17. CCR model for Line 02. a) Measured apparent resistivity pseudosection. b) Calculated apparent resistivity pseudosection. c) Recovered resistivity model. The erratic appearance of the pseudosections is an artefact of the contouring procedure.

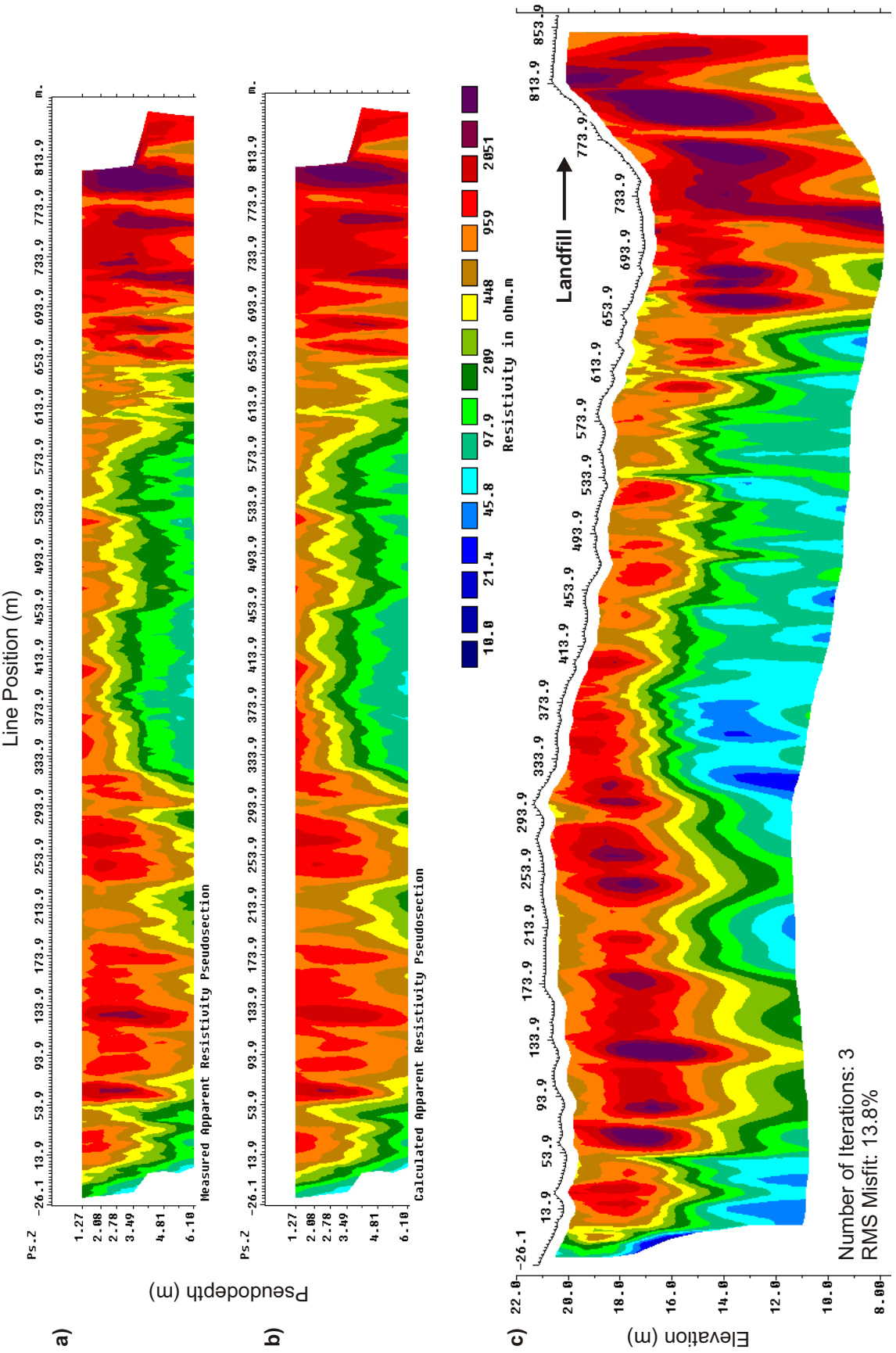

Figure 18. CCR model for Line 09. a) Measured apparent resistivity pseudosection. b) Calculated apparent resistivity pseudosection. c) Recovered resistivity model.

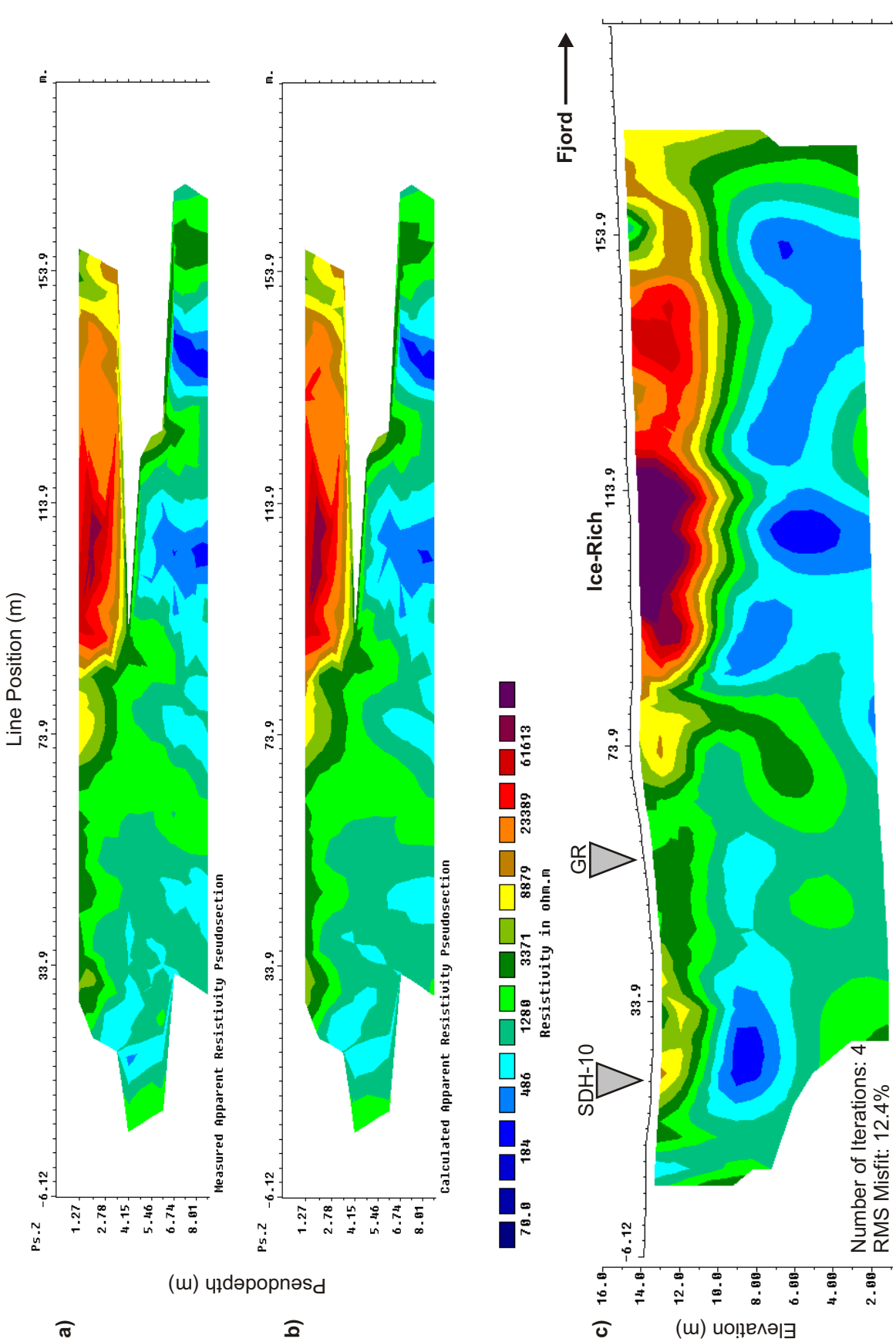

Figure 19. CCR model for Line 08. a) Measured apparent resistivity pseudosection. b) Calculated apparent resistivity pseudosection. c) Recovered resistivity model. Markers indicate the zero position of the corresponding GR model and the borehole location.

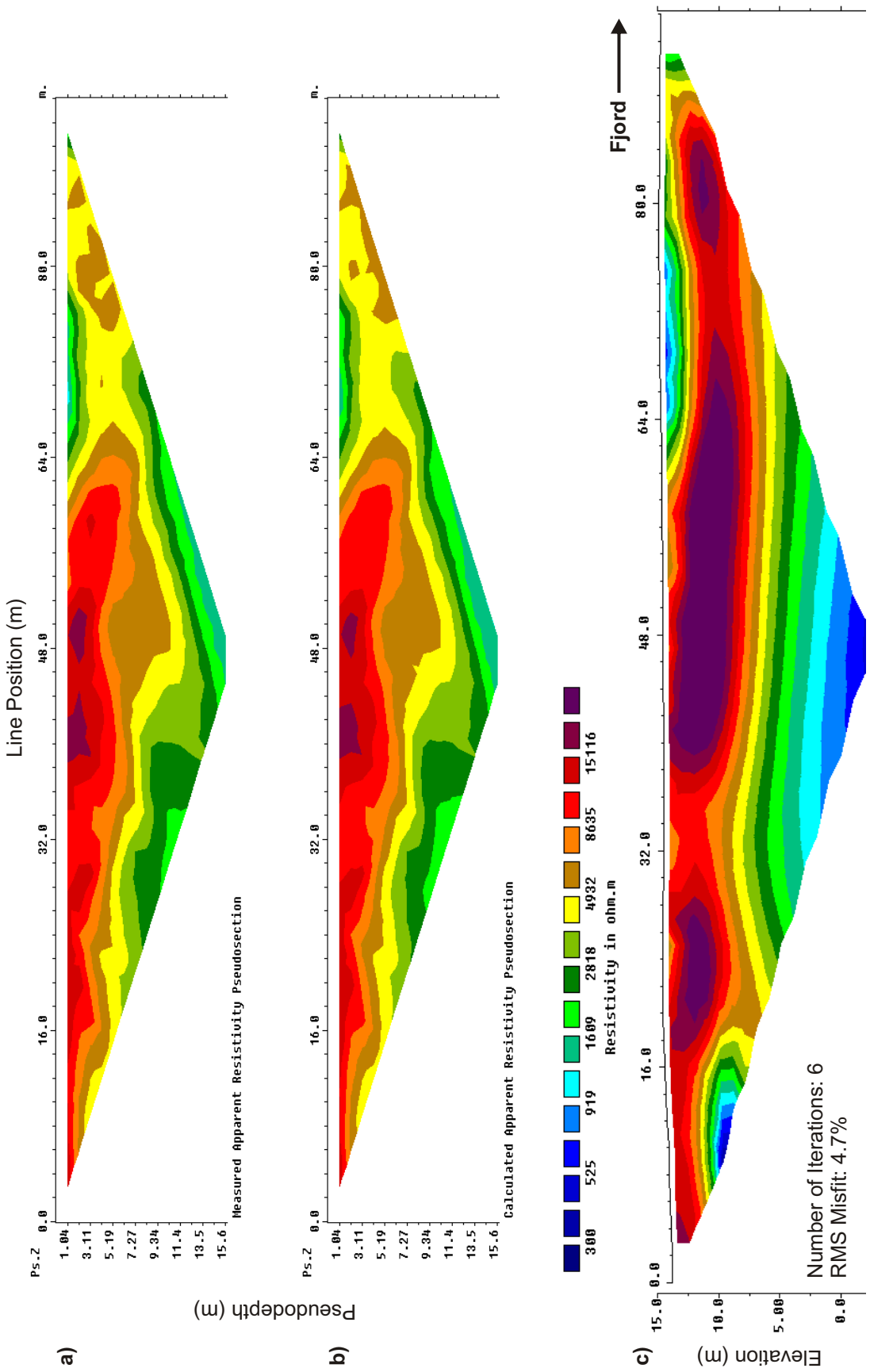

Figure 20. GR model for Line 08. a) Measured apparent resistivity pseudosection. b) Calculated apparent resistivity pseudosection. c) Recovered resistivity model.

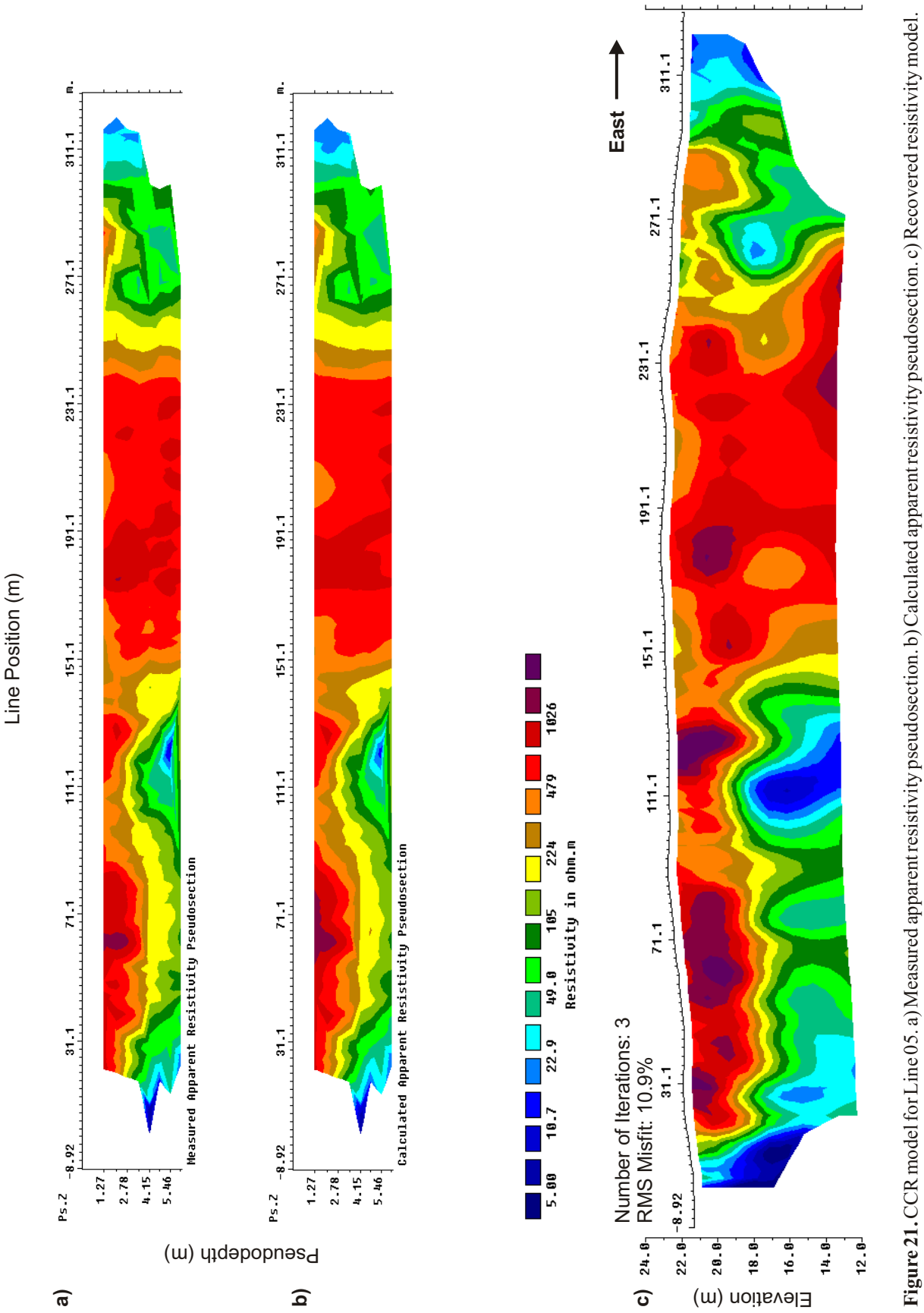

Figure 21. CCR model for Line 05. a) Measured apparent resistivity pseudosection. b) Calculated apparent resistivity pseudosection. c) Recovered resistivity model.

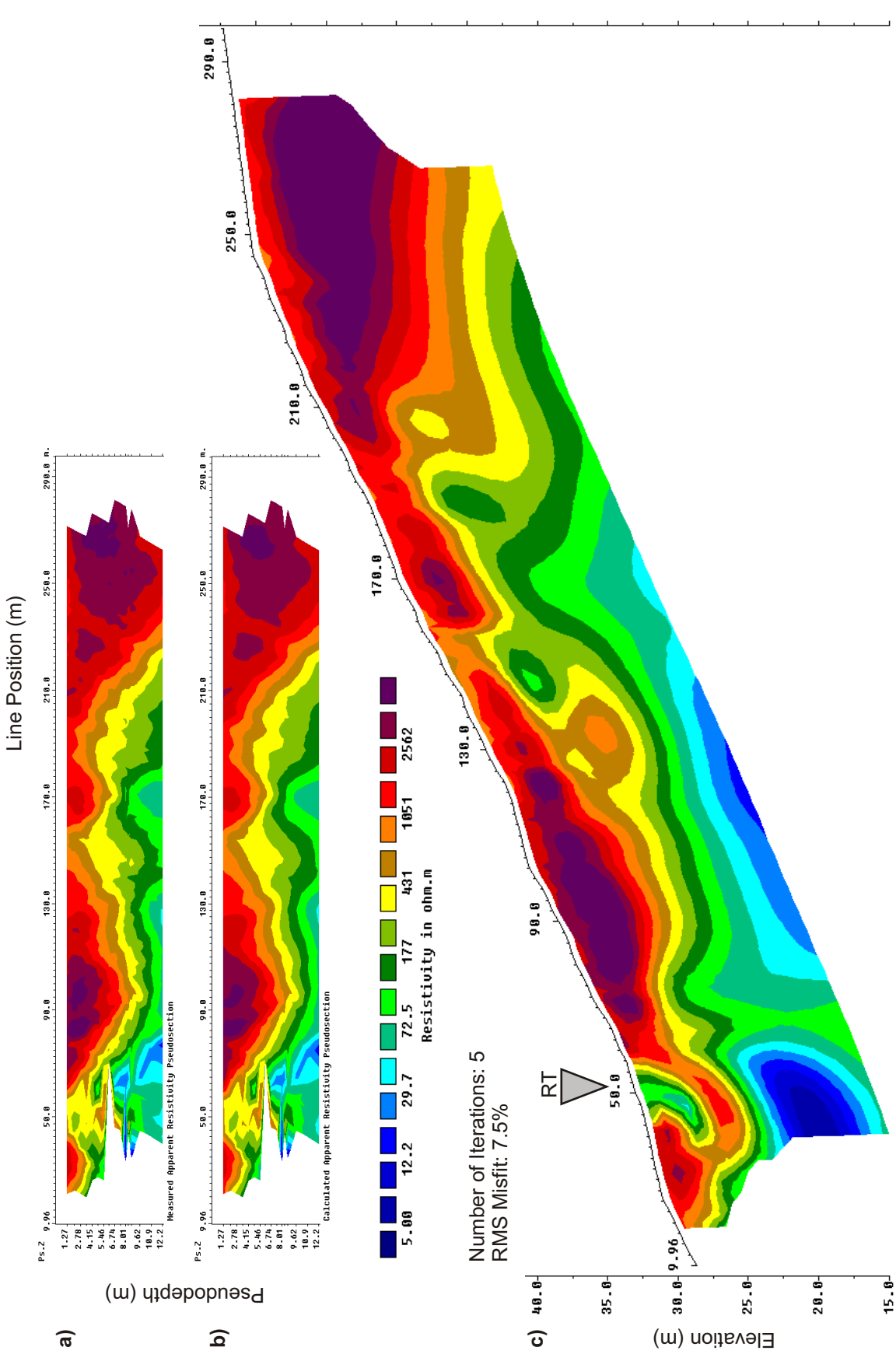

Figure 22. CCR model for Line 06. a) Measured apparent resistivity pseudosection. b) Calculated apparent resistivity pseudosection. c) Recovered resistivity model. Marker indicates the radio tower location.

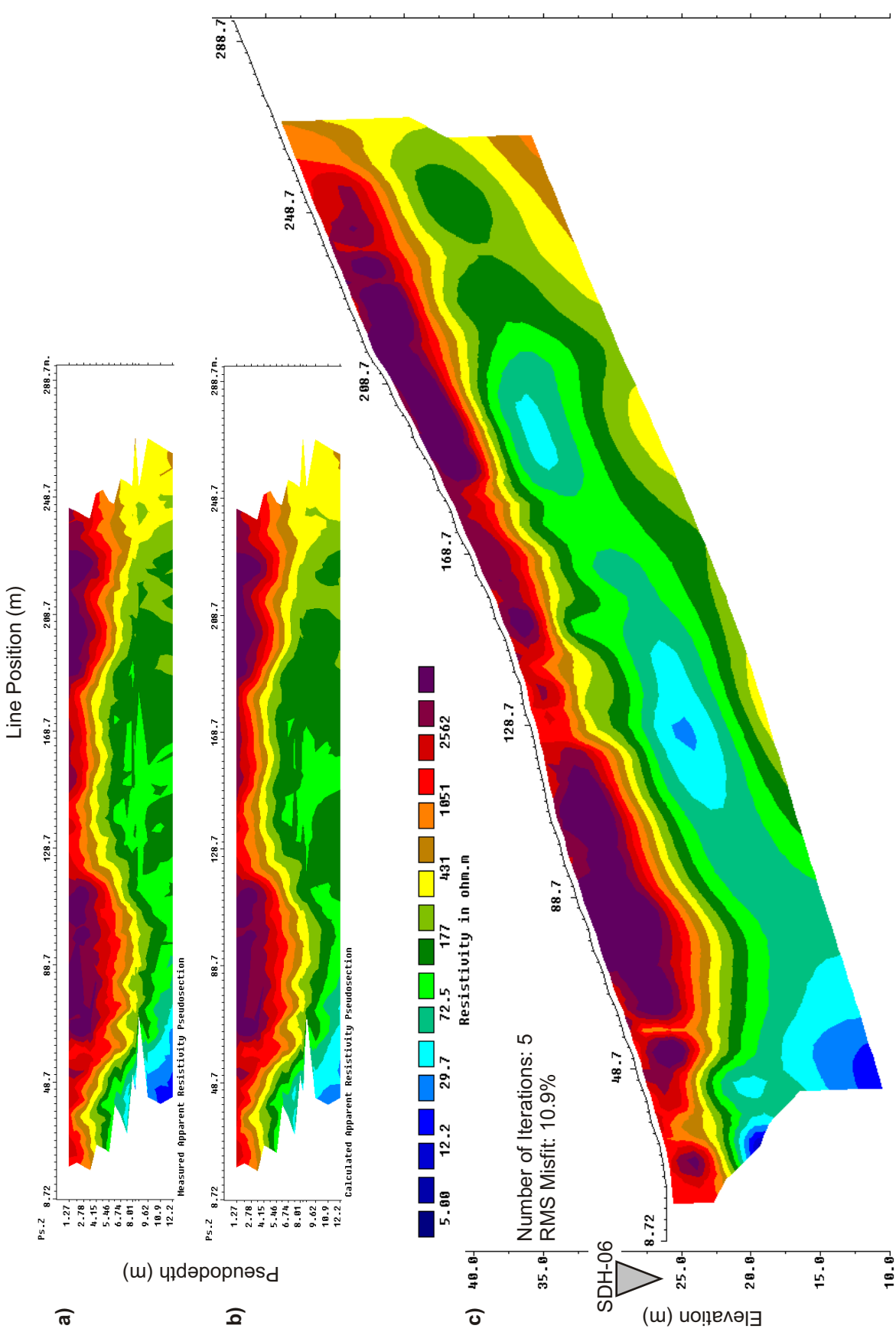

Figure 23. CCR model for Line 07. a) Measured apparent resistivity pseudosection. b) Calculated apparent resistivity pseudosection. c) Recovered resistivity model. Marker indicates the borehole location.